

Gravitational Wave Emission From Core-Collapse of Massive Stars

Chris L. Fryer

Theoretical Astrophysics, Los Alamos National Laboratories,
Los Alamos, NM 87544

Daniel E. Holz and Scott A. Hughes

Institute for Theoretical Physics, University of California, Santa Barbara, CA 93106

ABSTRACT

We derive estimates for the characteristics of gravitational radiation from stellar collapse, using recent models of the core-collapse of Chandrasekhar mass white dwarfs (accretion induced collapse), core-collapse supernovae and collapsars, and the collapse of very massive stars ($\gtrsim 300 M_{\odot}$). We study gravitational-wave emission mechanisms using several estimation techniques, including two-dimensional numerical computation of quadrupole wave emission, estimates of bar-mode strength, estimates of r-mode emission, and estimates of waves from black hole ringing. We also review the rate at which the relevant collapses are believed to occur, which has a major impact on their relevance as astrophysical sources. Although the latest supernova progenitor simulations produce cores rotating much slower than those used in the past, we find that bar-mode and r-mode instabilities from core-collapse supernovae remain among the leading candidate sources for LIGO-II. Accretion induced collapse (AIC) of a white dwarf could produce gravitational-wave signals similar to those from core-collapse. In the models that we examine, such collapses are not unstable to bar modes; we note that models recently examined by Liu and Lindblom, which have slightly more angular momentum, are certainly unstable to bar formation. Because AIC events are probably 1,000 times less common than core-collapse supernovae, the typical AIC event will be much further away, and thus the observed waves will be much weaker. In the most optimistic circumstances, we find it may be possible to detect gravitational waves from the collapse of $300 M_{\odot}$ Population III stars.

Subject headings: black hole physics—stars: black holes—stars: supernovae—
stars: neutron

1. Introduction

We are entering an age where gravitational-wave (GW) detectors will be sufficiently sensitive to observe a host of astrophysical sources. This has led to a flurry of activity among astrophysicists to estimate the characteristics of sources of GW emission. One source class that has been the subject of much study is the collapse of massive stars to form compact remnants (either neutron stars or black holes). Within this broad class, the collapse of supernova progenitors (typically $\sim 15 M_{\odot}$ stars) has received particularly strong scrutiny. Most studies have concentrated on calculating the GW emission during collapse, or the emission from bar-like instabilities shortly after bounce (see Rampp, Müller, & Ruffert 1998 for a review). However, the general class of stellar collapse includes a rather wide variety of astrophysical objects. Such objects range from the collapse of a white dwarf whose mass is pushed just beyond the Chandrasekhar limit via accretion (accretion induced collapse, or AIC; see Liu & Lindblom 2001) to the collapse of very massive stars, in excess of $260 M_{\odot}$ (Fryer, Woosley, & Heger 2001).

Although there is little doubt that stellar collapse produces GWs, it is difficult to accurately estimate the characteristics of the signal produced. The amount of radiation depends sensitively upon the rotation rate of the collapsing object. The choice of pre-collapse rotation can make a large difference in the resulting GW signal (Brown 2001), particularly in the case of bar-mode instability calculations in core-collapse supernovae.

Simulations generally suffer from two deficiencies. First, most collapse simulations use simplified equations of state that do not include the effects of neutrinos. Although neutrinos may not be important at early times (e.g., the simulations of Rampp et al. 1998), at later times they strongly affect the material dynamics and cannot be neglected. In this paper we take advantage of the results from a series of recent stellar-collapse simulations (Fryer et al. 1999a; Fryer & Heger 2000; Fryer et al. 2001) which followed stellar collapse to late times with realistic equations of state and neutrino physics.

Second, until recently no models of the progenitors of stellar collapse have included the effects of rotation, so that there has been little information available to constrain their initial spin. Recently, however, Heger (1998) has developed a stellar evolution code which includes a number of angular momentum transport processes and can evolve massive

stars to collapse. He found that the rotation speeds of collapsing supernova cores were much smaller than those used in most calculations of GW emission from core-collapse (e.g. Rampp et al. 1998). In this paper, we re-investigate the GW emission from stellar collapse using these latest progenitors in an effort to calculate a GW signal which more closely reflects what is produced in nature.

Our goal in this analysis is to make reasonable estimates for the GW strength from stellar collapse, and in particular to identify which scenarios lead to interesting GW sources for detectors such as LIGO. For each of the scenarios that we consider (accretion induced collapse, core-collapse supernovae, collapse of $M \gtrsim 300 M_{\odot}$ stars) we examine the GW emission from bulk mass motions, from mass currents, and from the “ringing” of a black hole (if one is produced). In this analysis we cannot precisely model GW production—our axisymmetric code cannot follow 3-dimensional instabilities, nor the complicated behavior for very long after collapse. We thus make a number of important assumptions and approximations to estimate GW characteristics, sufficient to accomplish the goal of this paper: to derive reasonable estimates for the frequency and strain of GW output.

GWs from mass motion are computed in three ways. First, we numerically evaluate the quadrupole moment and its rate of change from the axisymmetric simulations. These waves come from polar-type oscillations, and do not account for the instabilities caused by rotation. This axisymmetric estimate should strongly underestimate the GW emission from a source. Second, we assume the evolution of the system may lead to a bar-mode instability, and calculate the GW emission from the bar-mode that might develop. There are indications that the mass and angular momentum of some of our systems are in the range where secular, and perhaps dynamical, bar-mode instabilities develop. We estimate the bar GW strength over a range of evolutionary outcomes. Finally, as a physically motivated upper limit to GW production, we consider a fragmentation instability, wherein the star’s interior fragments into clumps. We model these clumps as a binary system. This binary is a rather strong radiator, and yields a reasonable upper bound on the GWs possible from a stellar source. It is not clear if such an instability would actually occur in a realistic collapse, but it has not been ruled out (Fryer et al. 2001). Indeed, we note that Van Putten (2001) has recently argued that a similar instability may be a source of copious GWs during long duration gamma ray bursts.

The r-mode instability produces GWs from mass currents. We estimate the r-mode wave characteristics following the approach of Ho & Lai (2000). This instability can be activated in a newly born, hot neutron star. It may also be reawakened when material falls back onto the neutron star after it has cooled—the fallback material heats and spins up the star.

In some evolutionary scenarios a black hole is formed. The nascent black hole is likely to be quite distorted from the quiescent Kerr form, and remains so as material falls back onto it in the first seconds or minutes of its life. This distortion drives the hole to radiate as it settles down to a Kerr state; the emitted waves are called “ringing” waves since they are qualitatively similar to the ringing of a bell. We estimate the strength and detectability of these waves using some simplifying assumptions about the distribution of infalling matter and the manner in which it distorts the hole.

In all cases we compare the expected wave strain from our sources with the noise in the broad-band configuration of enhanced LIGO interferometers (“LIGO-II”, see Gustafson et al. 1999). The comparison is based on a measure of the characteristic noise strain which assumes good knowledge of the source’s characteristics (“matched filtering”; see Appendix A for further details). It is worth noting that other data analysis techniques are likely to be very useful in searching for these waves (for example, the $f - \dot{f}$ technique of Van Putten & Sarkar (2000) would probably do very well at following the evolution of the black hole ringing frequency as its mass and spin evolve due to accretion). Since we are only interested in a first broad discussion of these waves, we do not consider these other data analysis techniques here.

LIGO is just one of several ground-based gravitational-wave interferometers currently planned or under construction. In Europe, a French-Italian collaboration is building the 3 kilometer VIRGO interferometer near Pisa, Italy (Marion 2000 and references therein). It will operate in the same time frame as LIGO, and is expected to have very similar noise characteristics. [One exception is that VIRGO will use a very sophisticated seismic isolation system that promises to move the low frequency noise “wall” from about 10 Hz (LIGO) to roughly 3 or 4 Hz.] A British-German collaboration is building the 600 meter GEO600 interferometer near Hannover, Germany (Lück et al. 2000 and references therein). One of GEO’s major goals is to use advanced interferometry techniques and technology from the beginning. As well as serving as a useful testbed for design ideas that will be used to improve LIGO and VIRGO, this design compensates for GEO’s shorter arms and enables it to achieve sensitivity comparable to that of the multi-kilometer instruments. In Japan, the TAMA collaboration is currently operating a 300 meter interferometer near Tokyo (Ando & Tsubono 2000 and references therein). This interferometer is being used as a testbed for a future multi-kilometer instrument with cryogenically cooled mirrors that they hope to build in the Kamioka mine (Kuroda et al. 2000). TAMA is of sufficient sensitivity to detect gravitational-wave events within the Milky Way and nearby galaxies. Finally, there are plans to build a LIGO-scale detector in western Australia, near Perth (McClelland et al. 2000). This would be a particularly valuable addition to the stable of detectors since the Northern Hemisphere detectors lie very nearly within a common plane.

An Australian detector would be far outside of this plane, allowing it to play an important role in determining the location of sources on the sky.

In the frequency band of greatest interest to this analysis ($f \gtrsim 100$ Hz or so), the different interferometers have sensitivities that are very similar to one another. Our discussion, which focuses on LIGO-II, carries over with little change to the other instruments. At low frequencies, VIRGO may have some advantage because of their aggressive seismic isolation design; in particular, they may have a better chance of detecting waves from the death of population III stars (which are at low frequencies because of the cosmological redshift). In any case, we provide enough information for the interested reader to compare our estimated wavestrains with the sensitivity of detectors other than LIGO-II.

The remainder of this paper is organized as follows. We review the various mechanisms that lead to GW emission in §2, and then apply them to collapse progenitors in §3 (AIC), §4 (core-collapse supernovae), and §5 (collapse of very massive stars). In each of these sections we review current constraints on collapse rates and discuss the detectability of the GWs. Background for the detectability discussion is reviewed in Appendix A. In several places we discuss sources at cosmological distances. To convert between redshift and luminosity distance (Hogg 1999), we assume a flat universe with $\Omega_m = 0.35$ and $\Omega_\Lambda = 0.65$, and with a Hubble parameter $h_{100} = 0.65$. (Bahcall et al. 1999). A summary of the results concludes the paper.

2. Gravitational Wave Emission Mechanisms

The collapse of massive stars involves a large amount of mass ($\sim 1\text{--}100 M_\odot$), in a fairly compact region ($\sim 10^8\text{--}10^9\text{cm}$), moving at relativistic velocities ($v/c \sim 1/5$)—precisely the conditions needed for strong GW generation. In what follows we will explore a number of GW emission mechanisms, including large-scale mass flows (quadrupole oscillations, bar-mode and fragmentation instabilities), large-scale mass currents (r-mode instability), and emission from the ringing of a newly-formed black hole. Each mechanism operates in a different regime, and the nature of GW emission depends sensitively upon the evolutionary development of the source. We will consider each mechanism in turn, discussing when each becomes important, and estimating the strength of the resulting gravitational radiation.

We begin with a very brief review of GW theory; further detail and references can be found in Thorne (1987). The conventional approach to calculating the GW emission of a given mass distribution is via a multipole expansion of the perturbation $h_{\mu\nu}$ to a background spacetime $g_{\mu\nu}^B$. The transverse-traceless projection of this metric, evaluated in the radiation

zone, is the metric of the radiation field. The lowest (quadrupole) order piece of this field is (Thorne 1980)

$$h_{jk}^{\text{TT}} = \left[\frac{2G}{d} \frac{d^2}{c^4 dt^2} \mathcal{I}_{jk}(t-r) + \frac{8G}{3d} \frac{G}{c^5} \epsilon_{pq(j} \frac{d^2}{dt^2} \mathcal{S}_{k)p}(t-r) n_q \right]^{\text{TT}}. \quad (1)$$

Here, \mathcal{I}_{jk} and \mathcal{S}_{jk} are the mass and current quadrupole moments of the source, d is the distance from the source to the point of measurement, ϵ_{ijk} is the antisymmetric tensor, and n_q is the unit vector pointing in the propagation direction. Parentheses in the subscripts indicate symmetrization over the enclosed indices, and the superscript TT indicates that one is to take the transverse-traceless projection; G is Newton’s gravitational constant, and c is the speed of light.

Most GW estimates are based on Eq. (1). When bulk mass motions dominate the dynamics, the first term describes the radiation. For example, this term gives the well-known “chirp” associated with binary inspiral. We will use it to model bar-mode and fragmentation instabilities. At least conceptually, this term also applies to black hole ringing, provided one interprets \mathcal{I}_{jk} as a moment of the spacetime rather than as a mass moment (Thorne et al. 1986). In practice, ringing waves are computed by finding solutions to the wave equation for gravitational radiation (Teukolsky 1973) with appropriate boundary conditions (radiation purely ingoing at the hole’s event horizon, purely outgoing at infinity; see Leaver 1985 for further discussion). The second term in Eq. (1) gives radiation from mass currents, and is used to calculate GW emission due to the r-mode instability.

When the background spacetime is flat (or nearly so) the mass and current moments have particularly simple forms. For example, in Cartesian coordinates the mass quadrupole is given by

$$\mathcal{I}_{jk} = \int d^3x \rho \left[x^j x^k - \frac{1}{3} r^2 \delta_{jk} \right], \quad (2)$$

where ρ is the mass density, and $\delta_{jk} = 1$ for $j = k$ and 0 otherwise. The second term in the integrand ensures that the resulting tensor is trace free.

Gravitational waves carry away energy and angular momentum from the source (Isaacson 1968). The lowest order contribution to the power P emitted in GWs is due to variations in the quadrupole moment:

$$P = \frac{dE}{dt} = \frac{1}{5} \frac{c^5}{G} \left\langle \ddot{\mathcal{I}}_{jk} \ddot{\mathcal{I}}_{jk} \right\rangle, \quad (3)$$

where the dots refer to time derivatives. For the purpose of detectability estimates, it is usually more important to know the dimensionless strain h associated with a source. This

strain gives the fractional change in distance between two separated masses as a GW passes by; it is the quantity that is directly measured by GW detectors. The tensor field h_{jk}^{TT} encodes two polarizations, h_+ and h_\times . These polarizations can be pulled out of h_{jk}^{TT} with appropriate projection operators (see Thorne 1987 for expressions and further discussion). The RMS strain associated with a source is then given by $h = \sqrt{\langle h_+^2 + h_\times^2 \rangle}$, where the angle brackets denote both an average over several wavelengths and an average over the sky. This RMS strain will be used in all of our analyses.

In general, the relation between strain and power scales as

$$P = \frac{\pi^2 c^3}{G} f^2 d^2 h^2, \quad (4)$$

where f is the GW frequency and d is the luminosity distance to the source. For a given strain, higher frequency waves radiate more energy. Because of detector noise, however, higher frequency waves are not necessarily more detectable.

In the remainder of this section we discuss five different approximation methods which are valid under varying conditions during stellar collapse. The first three (numerical quadrupole formalism, bar mode formation, fragmentation instability) can be used to get a handle on GW emission during the collapse itself, while the latter two (r-modes and black hole ringing) occur after the formation of a compact remnant.

2.1. Numerical quadrupole formalism

It is possible to directly apply Eq. (3) to the results of a numerical simulation. By evaluating the quadrupole moment on multiple time slices, one can compute the time derivatives numerically, and thereby determine the GW emission. Computing time derivatives across many slices, however, can generate an unacceptable amount of numerical noise. An alternate approach, based upon work by Blanchet et al. (1990), and used extensively by Zwerger & Müller (1997), rewrites the time derivatives as spatial derivatives, thereby avoiding the need to consider multiple time slices when calculating instantaneous power emission. Both the velocities of the particles and the Newtonian potential are known on a given slice. The gradient of the potential yields the forces acting on the particles, and, coupled with the velocity information, determines what the next slice will look like. Therefore, by utilizing the gradients directly, it is possible to calculate the GW emission while restricting oneself to a single numerical slice.

The expression we use to do this in the axisymmetric case comes from Zwerger & Müller (1997). The only non-vanishing quadrupole wave amplitude component, A_{20} , is

given by

$$A_{20}(t) = \frac{G}{c^4} \frac{16\pi^{3/2}}{\sqrt{15}} \int_{-1}^1 \int_0^\infty dr dz r^2 \rho \left[v_r^2(3z^2 - 1) + v_\theta^2(2 - 3z^2) - v_\phi^2 - 6v_r v_\theta z \sqrt{1 - z^2} - r \frac{\partial \Phi}{\partial r} (3z^2 - 1) + 3 \frac{\partial \Phi}{\partial \theta} z \sqrt{1 - z^2} \right]. \quad (5)$$

Spherical coordinates are used here, with $z = \cos\theta$; Φ is the Newtonian gravitational potential. The non-zero wave strain component is then given by $h_+ = \sqrt{(15/64\pi)} \sin^2\theta A_{20}/d$, where d is the luminosity distance to the source.

Although our code is axially symmetric (such that all the ∂_ϕ terms vanish), Eq. (5) still yields non-zero GW emission due to polar-type oscillations. These modes become important when there is large *aspherical* mass infall (or ejection). However, we would strongly underestimate GW emission if we restricted ourselves to these modes—emission should be much stronger in cases where the tangential motion of particles dominates the radial motion. We now discuss a number of non-axisymmetric modes which our code is unable to reproduce directly.

2.2. Bar modes

A bar mode instability is one of the more promising mechanisms by which a significant fraction of the collapsing system’s energy can be emitted in GWs. Bar mode instabilities occur in objects whose rotational kinetic energy exceeds some fraction of their potential energy, with the ratio generally written as $\beta \equiv T/|W|$. Standard lore (Chandrasekhar 1969) states that an object is unstable on a secular time scale if $\beta \gtrsim 0.14$, and is dynamically unstable if $\beta \gtrsim 0.27$. [We note, though, that recent work suggests that if the collapse hangs due to centrifugal forces producing a density profile which is not centrally peaked, dynamical instabilities can occur at a much lower value of β (Centrella et al. 2000).]

In most core-collapse simulations done with up-to-date progenitor models, it is found that the mass distribution does not become centrifugally hung up. This suggests that instability to bar mode formation might be unlikely: in these simulations, the density is centrally concentrated, and thus the low critical values of Centrella et al. (2000) do not apply. High values of β are necessary to induce bar-mode instabilities. Fortunately, the rotational energy can be very high in these models (Fig. 1), and it remains likely that bar-mode instabilities will occur.

Heartened by these results, we review here expressions describing bar mode GW emission. Consider a bar of mass m and length $2r$, rotating with angular frequency ω . The

GW energy radiated is given, in the quadrupole approximation, by

$$P_{\text{bar}} = \frac{32}{45} \frac{G}{c^5} m^2 r^4 \omega^6. \quad (6)$$

A detector at a distance d from the source would measure an rms strain

$$h_{\text{bar}} = \sqrt{\frac{32}{45} \frac{G}{c^4} \frac{m r^2 \omega^2}{d}}. \quad (7)$$

Note that, due to symmetry, the frequency of the emitted GWs is twice the bar’s rotation frequency.

2.3. Fragmentation instability

To set a physically motivated upper limit to the GW emission that might be produced in stellar collapse, we imagine that the collapse material fragments into clumps, which then orbit for some number of cycles as the collapse proceeds. For concreteness we consider the material fragmenting into a binary system, though it could very well fragment into more objects. We note that collapse simulations give some indication that this kind of instability may be present (Fryer et al. 2001). Also, Van Putten has recently argued that a fragmentation-type instability in collapsar powered gamma-ray bursts may drive very strong GW emission (Van Putten 2001).

For two bodies, each of mass m , in circular orbit about one another at a frequency ω and with separation $2r$, the power and mean strain are given by:

$$P_{\text{bin}} = \frac{128}{5} \frac{G}{c^5} m^2 r^4 \omega^6 \quad (8)$$

$$h_{\text{bin}} = \sqrt{\frac{128}{5} \frac{G}{c^4} \frac{m r^2 \omega^2}{d}}. \quad (9)$$

These results make no assumption about orbital frequency, and so apply to, for example, pressure supported as well as Keplerian orbits. For Keplerian orbits we have $4\omega^2 r^3 = Gm$, and the above expressions become

$$P_{\text{bin}} = \frac{2}{5} \frac{G^4}{c^5} \frac{m^5}{r^5} \quad (10)$$

$$h_{\text{bin}} = \sqrt{\frac{8}{5} \frac{G^2}{c^4} \frac{m^2}{r d}}. \quad (11)$$

Note that if the “horizons” of the two bodies touch ($r = 2mG/c^2$), then the power radiated reaches a maximum of $P = c^5/80G \sim 10^{57}$ ergs s⁻¹, independent of the mass of the system. The length of time such power emission is sustained, however, scales with the total mass (thus supermassive black hole binaries radiate more than microscopic ones).

2.4. R-modes

If the collapse forms a neutron star, an r-mode instability can arise at late times, once the neutron star has cooled. This instability has attracted much attention in the past few years, fueled by the discovery by Andersson (1998) and Friedman & Morsink (1998) that gravitational radiation drives r-mode instabilities in rotating neutron stars [see Lindblom (2001) for a review]. Unfortunately, an accurate calculation of GWs from the r-mode instability requires an understanding of the growth and maximum limit of the r-mode amplitude which, in turn, requires an understanding of the viscous terms that act to damp the modes (e.g., shear and bulk viscosities in the neutron star fluid, shear viscosities caused by crusts, magnetic viscosities, etc.). For instance, Rezzolla, Lamb, and Shapiro (2000) found that poloidal fields as low as 10^{10} G could damp out r-modes. These viscous terms depend upon the neutron star structure and equation of state. On top of these uncertainties, the GW signal depends upon the formation and evolution of young neutron stars (especially during the first 1000 s), and hence is subject to the various uncertainties associated with those processes.

For our study of GWs from r-modes, we use the simplified equations derived by Ho & Lai (2000), which consider only the dominant $l = m = 2$ mode with the initial neutron star structure from Owen et al. (1998): $M_{\text{NS}} = 1.4 M_{\odot}$, $R_{\text{NS}} = 12.53$ km (which follows from a polytropic equation of state with index $\Gamma = 2$). The spin frequency (ν_{S}) evolution of the neutron star from Ho & Lai (2000) is:

$$\frac{d\nu_{\text{S}}}{dt} = -2Q \frac{\nu_{\text{S}} \alpha^2}{\tau_{\text{V}}} \quad (12)$$

where the viscous timescale (τ_{V}) is given by:

$$\frac{1}{\tau_{\text{V}}} = \frac{T_9^{-2}}{2.52 \times 10^8} + \frac{T_9^6}{1.26 \times 10^9} \quad (13)$$

with $Q = 0.094$ and the neutron star temperature $T_9 = T/10^9$ K. For most of our calculations we assume that the temperature evolves with time under the prescription of Owen et al. (1998): $T_9 = (t/1 \text{ yr})^{-1/6}$. The r-mode amplitude α is driven by gravitational radiation and damped by viscous forces:

$$\frac{d\alpha}{dt} = -\frac{\alpha}{\tau_{\text{GR}}} - \frac{\alpha}{\tau_{\text{V}}}(1 - \alpha^2 Q) . \quad (14)$$

The gravitational radiation timescale (τ_{GR}) is given by:

$$\frac{1}{\tau_{\text{GR}}} = -\frac{1}{18.9 \text{ sec}} \left(\frac{\nu_{\text{S}}}{1 \text{ kHz}} \right)^6 . \quad (15)$$

With this prescription the r-mode amplitude would grow to very large values unless we set some critical amplitude. As in Ho & Lai (2000), if the mode amplitude rises above 1, we hold it constant and the spin evolution becomes:

$$\frac{d\nu_S}{dt} = -2 \frac{\nu_S \alpha^2}{\tau_V} \frac{\alpha^2 Q}{1 - \alpha^2 Q}. \quad (16)$$

Ho & Lai included the effects of magnetic breaking (via radiation from a dipole magnetic field) in the newly formed pulsar, and we discuss these effects in §§3 and 4.

We also examine the effect of fallback accretion onto the collapsed remnant. In core-collapse supernovae it is likely that $\gtrsim 0.1 M_\odot$ of material will fall back onto the newly formed neutron star $\sim 20 - 2000$ s after the explosion. The angular momentum of this fallback material leads to the formation of an accretion disk which spins up the neutron star as it accretes:

$$\frac{d\nu_S}{dt} \Big|_{\text{Fallback}} = \frac{dJ_{\text{Fallback}}/dt - 2\pi\nu_S dI/dt}{2\pi I}. \quad (17)$$

We assume that the angular momentum per unit mass accreted onto the star is equal to that of a Keplerian orbit at the neutron star surface:

$$\frac{dJ_{\text{Fallback}}}{dt} = \frac{dM_{\text{Fallback}}}{dt} \sqrt{GM_{\text{NS}}R_{\text{NS}}}. \quad (18)$$

We also assume that the change in the moment of inertia (I) is limited to the change in mass (the radius remains constant):

$$dI/dt = \frac{2\pi\nu_S I}{M_{\text{NS}}} \frac{dM_{\text{Fallback}}}{dt}. \quad (19)$$

This assumption is adequate to get the qualitative flavor of the accretion effects on GW emission from r-modes.

Typical fallback accretion rates for supernovae which produce neutron stars peak in the range $3 \times 10^{-4} - 3 \times 10^{-3} M_\odot \text{ s}^{-1}$ (Fryer, Colgate, & Pinto 1999b). Such high rates quickly smother any magnetic field, heating up the neutron star. The neutron star temperature is set by the temperature at the surface of the neutron star (Fryer et al. 1999b):

$$T_9 = 2.16 \times 10^3 S^{-1} \frac{10^6 \text{ cm}}{R_{\text{NS}}}, \quad (20)$$

where S is the entropy of the infalling material. For a $\Gamma = 4/3$ polytrope, this is given by (Fryer et al. 1999b):

$$S = 11.8 \left(\frac{M_{\text{NS}}}{M_\odot} \right)^{7/8} \left(\frac{M_\odot \text{ s}^{-1}}{dM/dt} \right)^{1/4} \left(\frac{10^6 \text{ cm}}{R_{\text{NS}}} \right)^{3/8} k_B \text{ per nucleon}. \quad (21)$$

Combining the equations for the evolution of the neutron star spin and the r-mode amplitude with Ho & Lai’s (2000) definition for the average wave amplitude $h(t)$ yields

$$h(t) = 1.8 \times 10^{-24} \alpha \left(\frac{\nu_s}{1\text{kHz}} \right) \left(\frac{20\text{Mpc}}{d} \right). \quad (22)$$

We use this formula to estimate r-mode GW emission in newly collapsed stars.

2.5. Black Hole Ringing

If the stellar collapse forms a black hole instead of a neutron star, a different mechanism produces GWs. The properties of the black hole during collapse rapidly change as material from the star falls onto it, increasing its mass and possibly its spin. The infalling matter also perturbs the hole’s geometry, distorting it from the Kerr solution. This distortion causes the hole to “ring” in distinct harmonics as gravitational radiation carries away the perturbation and the hole settles into a quiescent, stationary Kerr state.

An accurate calculation of this ringing would require a code that calculates the perturbation spectrum given a mass inflow. Here we take a much simpler approach, approximating the spectrum as a stochastic superposition of Kerr quasi-normal modes arising from repeated “thumping” by the matter flow onto the nascent black hole. Although this analysis is not adequate to rigorously detail the characteristics of the ringing waves emitted during massive star collapse, it should be adequate to estimate the waves’ strength and detectability. We hope to motivate more careful analyses that use inflow codes to compute the emitted waves (an early example of which is described in Papadopoulos & Font 2001).

A black hole distortion can be decomposed into spheroidal modes with spherical-harmonic-like indices l and m . The quadrupole modes ($l = 2$) presumably dominate, while the dominant m value depends upon the matter flow. The $m = \pm 2$ modes are bar-like, co-rotating (+) and counter-rotating (–) with the hole’s spin; the $m = \pm 1$ mode represents a shift of the black hole’s position; and the $m = 0$ mode is an axisymmetric distortion. For simplicity, we assume that the hole rings entirely in $m = 0$ and $m = 2$ modes. We exclude $m = \pm 1$ because it is difficult to estimate their importance without detailed calculations of the ringing spectrum, and we exclude $m = -2$ because it is likely to be strongly suppressed [it is counter to the spacetime’s rotation, and has an extremely short lifetime (see Chandrasekhar 1983, Fig. 45)]. We will vary the fraction of energy radiated in $m = 0$ and $m = 2$ waves to see how the detectability of these events varies with the nature of the hole’s distortion.

Each quasi-normal mode has a unique frequency f_{lm} and damping time τ_{lm} , depending only on the hole’s mass and spin (Leaver 1985). Useful fits to Leaver’s numerical data (see Leaver 1985, Tables 2 and 3; also Echeverria 1989), accurate to $\sim 10\%$, are

$$\begin{aligned} f_0 &\simeq 700 \text{ Hz} \left(\frac{20M_\odot}{M} \right) [1 - 0.13(1 - a/M)^{6/10}] , \\ Q_0 &\simeq 3 - (1 - a/M)^{4/10} ; \end{aligned} \tag{23}$$

$$\begin{aligned} f_2 &\simeq 1600 \text{ Hz} \left(\frac{20M_\odot}{M} \right) [1 - 0.63(1 - a/M)^{3/10}] , \\ Q_2 &\simeq 2(1 - a/M)^{-9/20} . \end{aligned} \tag{24}$$

The quality factor $Q \equiv \pi f \tau$. We have suppressed the l subscript since it is 2 in all cases.

The amplitude of the ringdown waves, and the energy that they carry, depends upon the manner and extent to which the hole is distorted. A useful starting point is the “DRPP” result (Davis et al. 1971): the total energy carried off by GWs when a mass μ falls radially onto a Schwarzschild black hole of mass M is

$$\Delta E_{\text{DRPP}} = 0.01 \mu c^2 (\mu/M) . \tag{25}$$

For a rotating hole, this formula underestimates the energy radiated for matter falling down the poles by a spin-dependent factor $\lesssim 50\%$ (Sasaki & Nakamura 1982). Also, it only applies to an $m = 0$ perturbation—the energy radiated from a non-axisymmetric perturbation could be significantly larger. We will assume that Eq. (25) correctly describes the scaling of ΔE with μ , but will allow the size of ΔE to vary with a parameter ε :

$$\Delta E = \varepsilon \mu c^2 (\mu/M) . \tag{26}$$

From the energy emitted, ΔE , we estimate the GW amplitude associated with a single clump falling into the hole. The energy flux carried by GWs is (Isaacson 1968):

$$\frac{dE}{dAdt} = \frac{c^3}{16\pi G} \overline{\left[\left(\frac{\partial h_+}{\partial t} \right)^2 + \left(\frac{\partial h_\times}{\partial t} \right)^2 \right]} . \tag{27}$$

(The overbar indicates that this expression must be averaged over several cycles or wavelengths.) Quasi-normal ringing waves are damped sinusoids, so the waveform for a combination of $m = 0$ and $m = 2$ waves can be written

$$\begin{aligned} h_+(t) &= [\mathcal{A}_0 S_{20}(\theta, \phi; a) e^{-t/\tau_0} \cos(2\pi f_0 t + \varphi_0) + \mathcal{A}_2 S_{22}(\theta, \phi; a) e^{-t/\tau_2} \cos(2\pi f_2 t + \varphi_2)] / D, \\ h_\times(t) &= [\mathcal{A}_0 S_{20}(\theta, \phi; a) e^{-t/\tau_0} \sin(2\pi f_0 t + \varphi_0) + \mathcal{A}_2 S_{22}(\theta, \phi; a) e^{-t/\tau_2} \sin(2\pi f_2 t + \varphi_2)] / D, \end{aligned} \tag{28}$$

where D is the luminosity distance from the distorted hole, θ and ϕ are angles on the sky, the functions $S_{20}(\theta, \phi; a)$ and $S_{22}(\theta, \phi; a)$ are spheroidal harmonics [reducing to spherical harmonics when the black hole is not spinning ($a = 0$)], and (φ_0, φ_2) are phase offsets, related to the initial perturbation of the hole.

Plugging Eq. (28) into Eq. (27) and integrating over a large sphere gives

$$\frac{dE}{dt} = \frac{c^3 \pi}{G 4} [\mathcal{A}_0^2 f_0^2 e^{-2t/\tau_0} + \mathcal{A}_2^2 f_2^2 e^{-2t/\tau_2}] . \quad (29)$$

We have used the fact that the spheroidal harmonics are orthonormal functions on the sphere, and we have approximated $2\pi f \gg 1/\tau$ (which introduces errors of $\sim 10\%$). Integrating over time and using the definition of Q yields

$$\begin{aligned} \Delta E &= \frac{c^3}{8G} [Q_0 f_0 \mathcal{A}_0^2 + Q_2 f_2 \mathcal{A}_2^2] , \\ &\equiv \Delta E_0 + \Delta E_2 . \end{aligned} \quad (30)$$

We equate this ΔE to that given by Eq. (26). Since we do not know how to apportion this energy among the $m = 0$ and $m = 2$ modes, we split it up with a parameter α_{ring} :

$$\Delta E_0 = \alpha_{\text{ring}} \Delta E , \quad \Delta E_2 = (1 - \alpha_{\text{ring}}) \Delta E . \quad (31)$$

In principle, α_{ring} could be time dependent—for instance, it will increase if the mass inflow becomes axisymmetric later in the collapse. We ignore this possibility here, and take α_{ring} to be constant. We finally obtain

$$\begin{aligned} \mathcal{A}_0 &= \sqrt{\frac{8G\alpha_{\text{ring}}\Delta E}{Q_0 f_0 c^3}} = \sqrt{\frac{8\varepsilon G\alpha_{\text{ring}}\mu^2}{Q_0 c M f_0}} , \\ \mathcal{A}_2 &= \sqrt{\frac{8G(1 - \alpha_{\text{ring}})\Delta E}{Q_2 f_2 c^3}} = \sqrt{\frac{8\varepsilon G(1 - \alpha_{\text{ring}})\mu^2}{Q_2 c M f_2}} . \end{aligned} \quad (32)$$

To set an upper limit on the strength of the emitted waves, we assume that the accretion flow is extremely clumpy: the hole gets “thumped” by a clump of mass $\mu = \dot{m}T_{\text{thump}}$ every T_{thump} . The thump time T_{thump} will be treated as a variational parameter: for example, when it is very large, the ringdown signal consists of a small number of very large thumps. The amplitudes for a single thump are

$$\begin{aligned} \mathcal{A}_0 &= \sqrt{\frac{8\varepsilon G}{c} \frac{\dot{m}T_{\text{thump}}}{M^{1/2}}} \left(\frac{\alpha_{\text{ring}}}{Q_0} \right)^{1/2} , \\ \mathcal{A}_2 &= \sqrt{\frac{8\varepsilon G}{c} \frac{\dot{m}T_{\text{thump}}}{M^{1/2}}} \left(\frac{1 - \alpha_{\text{ring}}}{Q_2} \right)^{1/2} . \end{aligned} \quad (33)$$

We define the time index k via $t_k = kT_{\text{thump}}$. By stringing together a sequence of thumps and averaging over sky position, we finally arrive at the following expression for the gravitational waveform:

$$\begin{aligned}
 h(t) \equiv h_+(t) - ih_\times(t) &= \frac{\sqrt{2\varepsilon G/\pi c}}{D} \sum_{k=0}^{k_{\text{max}}} \frac{\dot{m}(t_k)T_{\text{thump}}}{M(t_k)^{1/2}} \times \\
 &\quad \left[\left[\frac{\alpha_{\text{ring}}}{Q_0(t_k)} \right]^{1/2} e^{-(t-t_k)/\tau_0(t_k)} e^{-2\pi i f_0(t_k)(t-t_k)} e^{-i\varphi_0(t_k)} \right. \\
 &\quad \left. + \left[\frac{1 - \alpha_{\text{ring}}}{Q_2(t_k)} \right]^{1/2} e^{-(t-t_k)/\tau_2(t_k)} e^{-2\pi i f_2(t_k)(t-t_k)} e^{-i\varphi_2(t_k)} \right].
 \end{aligned} \tag{34}$$

All functions which evolve with time are written explicitly as functions of t_k . Note in particular the phases $\varphi_0(t_k)$ and $\varphi_2(t_k)$: because they depend upon the distortion state of the hole as each clump arrives and further distorts the horizon, they will be random for all practical purposes. Thus the ringing waves emitted from the mass inflow will be stochastic. The index k_{max} describes the time at which the accretion flow ends and the hole stops ringing.

Equation (34) will be coupled with descriptions of the mass flow in later sections of this paper to estimate the detectability of these waves.

Having finished our discussion of relevant GW emission mechanisms, in the next three sections we turn to a number of possible astrophysically relevant GW sources.

3. Accretion Induced Collapse

When a white dwarf’s mass exceeds the Chandrasekhar limit¹, it begins to collapse. As it contracts, its temperature increases adiabatically. Neutrino cooling (via Urca processes) limits the rise in temperature. If neutrino cooling does not reduce the adiabatic heating significantly, the collapsing white dwarf will reach temperatures hot enough to ignite nuclear burning. The entire white dwarf explodes in a thermonuclear explosion known as a Type Ia supernova. If, on the other hand, cooling initially prevents nuclear ignition, the white dwarf

¹By Chandrasekhar limit, we mean the maximum mass of a stable white dwarf. Note that this depends upon composition and angular momentum.

will collapse more and more quickly as electrons capture onto protons, and the white dwarf will ultimately form a neutron star.

This “Accretion-Induced Collapse” (AIC) of a white dwarf is very similar to core-collapse supernovae. The collapse of white dwarfs has been studied in some detail over the past few decades (Hillebrandt, Wolff, & Nomoto 1984, Woosley & Baron 1992, Fryer et al. 1999a), and we have some understanding of the collapse process and the resultant explosion. Since the white dwarf is pushed over the Chandrasekhar mass limit through disk accretion, it is likely that the collapsing white dwarf will rotate at a significant rate, allowing for the possibility of a variety of instabilities, and the concomitant emission of GWs. The analysis in this paper relies upon the rotating simulation (model 3) of Fryer et al. (1999a).

3.1. Formation Rate and Angular Momentum

Calculating the formation rate of AICs from first principles is fraught with difficulties, ranging from understanding binary star evolution to uncertainties in the accretion process itself. We have already mentioned one such uncertainty: Does the star ignite in a thermonuclear explosion or collapse to form an AIC? At present we have only a rudimentary understanding of the conditions necessary for a white dwarf to gain matter during the accretion process (as opposed to losing matter via a series of nova explosions). Fortunately, due to the importance of Type Ia supernovae as cosmological candles, there has been a lot of activity studying the progenitor evolution and mass accretion necessary to produce Chandrasekhar-massed white dwarfs (see Nomoto, Iwamoto, Kishimoto 1997; Branch 1998; or Livio 2000 for reviews). Unfortunately, whether or not the current mass-transfer progenitors actually lead to an increase in the white dwarf mass to the Chandrasekhar limit is still a matter of hot debate (contrast Kato & Hachisu 1999 with Cassisi, Iben & Tornambé 1998). All of the uncertainties in binary evolution, accretion, etc. make it difficult at this time to directly calculate the formation rate of Chandrasekhar-mass white dwarfs.

We therefore rely upon indirect methods to place constraints on the AIC rate. One way is to derive a rate of thermonuclear explosions from Chandrasekhar-massed white dwarfs and calculate the *relative* fraction of Chandrasekhar-massed white dwarfs which produce AICs. Calculating relative rates removes some portion of the uncertainties, and may be easier to estimate theoretically. It is becoming increasingly evident that the thermonuclear explosion of a Chandrasekhar-massed white dwarf is the mechanism which produces Type Ia supernovae (Nomoto, Iwamoto, & Kishimoto 1997; Branch 1998; or Livio 2000). From observations of Type Ia supernovae, we infer a minimum rate at which Chandrasekhar-massed white dwarfs are produced in the Galaxy: $4 \pm 1 \times 10^{-3} \text{ yr}^{-1}$

(Cappellaro et al. 1997). Some fraction of Chandrasekhar-massed white dwarfs will collapse to form a neutron star. Which fate befalls the white dwarf depends sensitively upon the initial mass of the white dwarf, its chemical composition, and the rate at which it accretes matter (see Nomoto & Kondo 1991 for review). Although calculating this fraction may be easier than calculating a rate directly, at present we are unable to make accurate estimates.

By modeling the collapse itself, however, we can place constraints on the AIC rate. During the collapse the white dwarf ejects the outer $\sim 0.1 M_{\odot}$ of its envelope, some of which had become very neutron rich due to electron capture. As this material is ejected, it “pollutes” the Galaxy with extremely rare, neutron-rich isotopes. By measuring the total amount of these isotopes in the Galaxy, and assuming these isotopes are formed solely in AICs, we can place an upper limit on the rate of AICs in the Galaxy at about 10^{-5} per year (Fryer et al. 1999a).

What about the angular momentum distribution of these collapsing stars? The white dwarf is pushed above the Chandrasekhar mass either by accretion or through the merger of two white dwarfs. In either case the process by which the white dwarf gains mass also causes the white dwarf to gain a considerable amount of angular momentum. One can roughly estimate the rate of angular momentum gain by assuming all of the angular momentum at the inner edge of the accretion disk is added to the white dwarf:

$$\dot{J} = \dot{m} \sqrt{GM_{\text{WD}} R_{\text{disk}}}, \quad (35)$$

where \dot{m} is the accretion rate, G is the gravitational constant, M_{WD} is the mass of the white dwarf, and R_{disk} is the inner radius of the accretion disk. A 2500 km, $1.35 M_{\odot}$ white dwarf (with R_{disk} set to the white dwarf radius) accreting $0.05 M_{\odot}$ gains $2 \times 10^{49} \text{ g cm}^2 \text{ s}^{-1}$ in angular momentum. Given the small moment of inertia of white dwarfs (typically, $I/M_{\text{WD}} R_{\text{WD}}^2 < 0.1$), this small amount of accretion can cause an initially non-rotating neutron star to achieve rotation rates greater than 1 rad s^{-1} , or periods less than 6 s. It should be noted, though, that rotation periods for cataclysmic variables typically range from 200–1200 s (Liebert 1980) [although periods as low as ~ 30 s exist (King & Lasota 1991)]. Most white dwarfs lose mass during accretion due to novae, and this may limit the amount of angular momentum accreted (e.g. King, Wynn, & Regev 1991). It is possible that those white dwarfs which actually gain mass up to the Chandrasekhar mass may have much faster spin periods than the observed sample. Even so, the actual spin period before collapse depends upon a variety of uncertainties: white dwarf radius, accretion rate, magnetic field strength, etc. (e.g. Narayan & Popham 1989). For the purposes of our analysis, we assume that the white dwarf collapsed with $J = 10^{49} \text{ g cm}^2 \text{ s}^{-1}$ (Fig. 2). Liu & Lindblom (2001) have recently studied white dwarfs with more angular momentum ($J = 3\text{--}4 \times 10^{49} \text{ g cm}^2 \text{ s}^{-1}$), and we will compare our results with theirs below.

3.2. Gravitational Waves

3.2.1. *GW from Collapse or Explosion*

As we discussed in §2, bar-mode instabilities are driven when the ratio of rotational kinetic energy to potential energy (β) exceeds some critical value. Toroidal density distributions (where the density peaks some distance away from the center of the object) are more susceptible to bar-mode instabilities, and may develop these instabilities for $\beta \gtrsim 0.10 - 0.12$ (Tohline & Hachisu 1990; Centrella et al. 2000). The collapse of a rotating white dwarf does produce a density distribution peaked away from the center (Fig. 3), and the critical β may be as low as Tohline & Hachisu (1990) predict. However, for our choice of initial spin, β is less than 0.06. For AICs, the boundary between proto-neutron star and ejected material is generally very sharp, but in core-collapse supernovae it is sometimes difficult to define the edge of the proto-neutron star. Hence we have calculated β as a function of enclosed mass, where β corresponds to the total rotational energy and potential energy in that enclosed mass. Note that no matter where we define the edge of the neutron star, $\beta < 0.06$. That said, we should bear in mind that the higher angular momentum white dwarfs of Liu & Lindblom (2001) are almost certainly unstable.

Polar-type oscillations estimated from the quadrupole formula (§2.1) predict a peak strain of 5.9×10^{-24} at 100 Mpc and GW energies of 3×10^{45} ergs (see Table 1). These waves are emitted at a frequency of about 50 Hz. The RMS noise strain of LIGO-II broad-band interferometers (cf. Appendix A) is about 6×10^{-23} near 50 Hz. The strength of these waves is an encouraging sign that, *if* stronger instabilities such as bar mode formation were to become active, they would likely be of great observational importance (though these polar observations are not themselves observationally interesting).

3.2.2. *GW from Remnants*

For the first 10–20 s after collapse and explosion from the AIC, the proto-neutron star remnant remains electron rich. Electron neutrinos (created via electron capture onto protons) deleptonize the neutron star, but since the degeneracy energy of electrons is less than the energy carried away by the neutrinos (that is, the energy released through electron capture is more than the energy carried away by the neutrinos produced in electron capture), the neutron star initially heats up (Keil & Janka 1995). It can take up to 50 s before the temperature falls below 10^{10} K. By this time the proto-neutron star has contracted to nearly its final radius. Assuming a $1.4 M_{\odot}$, 12.53 km neutron star ($\Gamma = 2$ polytrope), the moment of inertia is only 1.1×10^{45} g cm². As long as the total angular

momentum is above $7 \times 10^{48} \text{ g cm}^2 \text{ s}^{-1}$, the period will be below 1 ms, and the neutron star remnant will be an ideal candidate for strong r-mode emission. However, r-modes are highly damped until the temperature (and hence the bulk viscosity) decreases below 10^{10} K . In our analysis, we assume the neutron star has contracted after 10 s and using $T_9 = (t/1 \text{ yr})^{-1/6}$, $T_9 = 12$ at this time. As the proto-neutron star cools, the r-mode amplitude grows and converts much of the rotational energy into GW emission (Fig. 4; solid line). To compare with Ho & Lai (2000), we have assumed a spin frequency set to 890 Hz. If instead the neutron star is initially much hotter, but cools faster ($T_9 = (t/1 \text{ yr})^{-1/3}$), the GW signal occurs later, but the strength and rough structure is nearly the same (Fig. 4; dot-dashed line). The total energy emitted in GWs exceeds 10^{52} ergs with a maximum power of over $10^{50} \text{ ergs s}^{-1}$ (Table 1).

AIC r-mode waves are compared to LIGO’s mean noise in the lower track of Figure 5 (see Appendix A for discussion of how this track is calculated, and Owen et al. (1998) for further discussion). The track illustrates the strength of the waves if it were possible to coherently integrate the signal’s phase evolution over the course of 1 year. The wave track is below the mean noise everywhere on the plot, indicating that these waves are not detectable. This is not too surprising, since one typically discusses r-mode strength for sources no more than about 20 Mpc away — 100 Mpc is just too far for the source to be detectable.

The above calculations assume that the neutron star has also acquired a 10^{12} G dipole magnetic field and is emitting as a pulsar (however, we neglect any damping effects caused by magnetic fields). In the first year, a total of $2 \times 10^{47} \text{ ergs}$ is lost through pulsar emission, most of which will power the accelerated ejection of the exploding material. This energy is less than 0.1% of the explosion energy, and only 0.001% of the total rotation energy. Although this energy will not make a difference in the supernova light curve at early times, the pulsar luminosity remains high long after the supernova and GW emission has died away, and will easily be visible after the ejecta has cleared. A 10^{13} G magnetic field pulsar is similar ($E_{\text{Pulsar,1yr}} = 2 \times 10^{49} \text{ ergs} = 2\% E_{\text{explosion}} = 0.1\% E_{\text{GW}}$). At 10^{14} G , the pulsar mechanism will produce observable effects in the supernova explosion at peak, even though less than 10% of the rotational energy is going into pulsar emission. If AICs do produce such highly magnetized, rapidly rotating stars, we should observe the pulsar outbursts.² Unfortunately, at a rate of 10^{-5} per year in the Galaxy, we only expect 0–1 such events in our current sample of supernovae.

²We assume that the dipole magnetic field mechanism for pulsars works in these conditions

4. Core-Collapse Supernovae

Stars more massive than $\sim 8 M_{\odot}$ also end in core-collapse. During their lives successive stages of nuclear burning build up a massive iron core in the stellar center. This iron core is supported by electron degeneracy and thermal pressures. When the density and temperature in the core become so high that iron is dissociated into alpha particles and electron capture occurs, the support pressure is suddenly removed and the core collapses. As it collapses, the core density and temperature increases, causing more iron dissociation and electron capture which leads to a runaway infall of the core. Just as with AICs, the core collapses until it reaches nuclear densities, where nuclear forces and neutron degeneracy pressure abruptly halt the collapse.

Astronomers have long understood that the potential energy released as a star collapses down to a neutron star could power a supernova explosion (Baade & Zwicky 1934). However, it was not until 1966 that Colgate & White realized that neutrinos could be the medium which transported energy released during the collapse of the core into the outer layers of the star, which would subsequently explode and drive the supernova explosion. Since this time astronomers have continued to refine the neutrino-driven model. Indeed, core-collapse supernovae are one of the few objects in astronomy that astronomers do not invoke fudge factors to explain (albeit, this means that we do not yet match the observations all that well).

The basic mechanism behind core-collapse supernovae has developed from three decades of study and is very similar to AICs. The main difference arises from the fact that the proto-neutron star must somehow eject $\gtrsim 10 - 15 M_{\odot}$ of material, instead of $0.1 M_{\odot}$ as in the case of AICs. After bounce, the inner portion of the star rains down upon the proto-neutron star, preventing a quick, AIC-like explosion. A convective layer above the proto-neutron star and below the pressure cap of the infalling material converts the heat deposited by neutrinos into kinetic energy, aiding the explosion. Eventually, the energy in the convective layer is sufficient to overcome the ram pressure and a supernova explosion is launched.

As the mass of the collapsing star increases, the basic picture described above of core-collapse supernovae begins to change. Above $20-25 M_{\odot}$, the supernova explosion is too weak to eject the entire star, and much of the star ($> 2 M_{\odot}$) falls back onto the neutron star $100-100,000$ s after the supernova explosion (and after the GW emission). This fallback matter pushes the remnant mass above the maximum neutron star mass, and it collapses to form a black hole. Beyond $\sim 40-50 M_{\odot}$, the convective layer is unable to overcome the pressure of the infalling material. No supernova explosion is launched and the star collapses to form a black hole. These direct-collapse stars will differ from normal core-collapse

simulations in both GW emission and optical output. They are known as “collapsars”, and constitute one of the favored models for gamma-ray bursts (Woosley 1993). Unfortunately, beyond $\sim 40\text{--}50 M_{\odot}$, mass-loss from stellar winds can dramatically change the mass of the star before collapse, and it may be that nature does not produce any high-metallicity collapsar progenitors.

4.1. Formation Rate and Angular Momentum

The formation rate of core-collapse supernovae is fairly well known, and lies somewhere between 1 per 50–140 years in the Galaxy (Cappellaro et al 1997). 5–40% of these supernovae produce black holes through fallback accretion (Fryer & Kalogera 2001). Because mass-loss from winds are uncertain, the fraction of massive stars which collapse directly into black holes is much less well determined (Fryer & Kalogera 2001). And for all core-collapse models, we do not know the fraction of these massive stars (if any) that are rotating rapidly enough to emit detectable amounts of GWs.

One way to get a handle on the angular momentum is to study pulsars, the compact remnants of core-collapse supernovae. From measurements of young pulsars we know that at least some neutron stars are born with periods faster than 20 ms. But whether or not any neutron stars are born with millisecond periods is hard to ascertain. The problem is that pulsars spin down as they emit radiation, but we don’t know exactly how fast the spin-down occurs. The most recent analysis by Chernoff & Cordes (private communication) found that they could fit the initial spin periods with a Gaussian distribution peaking at 7 ms with sub-ms pulsars lying beyond the 2-sigma tail. Does this mean that less than 10% of pulsars are born spinning with millisecond periods, or does it mean that many pulsars are born spinning rapidly and GW emission removes a considerable amount of their angular momentum? In addition, the analysis of Chernoff & Cordes is very sensitive to their choice of spin down rates and other uncertainties in their population study, and they stress that such results should be taken with a great deal of caution.

Stellar theorists have now produced models of core-collapse progenitors which include angular momentum (Heger 1998). Although these simulations include a number of assumptions about the angular momentum transport in the massive star, they give us some handle on the angular momentum distribution in the collapsing core. We base our analysis on the angular momentum profiles from the core-collapse simulations of Fryer & Heger (2000), which uses these latest progenitors and modeled the core-collapse through supernova explosion (Models 1,5; Fig. 2). The angular momentum in these collapsing cores is much less than what is typically used in GW calculations, and we’ll discuss the differences in the

results below.

4.2. Gravitational Waves

4.2.1. GW from Collapse or Explosion

Because the angular momentum distributions used by Fryer & Heger (2000) have peak values significantly lower than those used in the past, there is no centrifugal hang-up. The collapse proceeds nearly identically to a non-rotating star, with a density distribution peaked at the center of the star (Fig. 3). This makes it harder for bar-mode instabilities to develop and produces weaker GW emission. During bounce, the neutron star is not compact enough to quickly drive bar-mode instabilities. However, Fryer & Heger (2000) found that the explosion produced by these rotating core-collapse supernovae is much stronger along the poles than along the equator, causing more of the low angular-momentum material to be ejected. Hence, after the explosion (~ 1 s after collapse), β can increase to high enough values that bar-mode instabilities are likely to develop (Fig. 1). The proto-neutron star extends in all cases beyond $\sim 1 M_{\odot}$, corresponding to values of β which are certainly above the secular instability limit and probably above the dynamic instability limit (see §2.2). Notice in Fig. 1 that β is actually larger for the model which has less angular momentum. This is because this model has contracted more and is spinning more rapidly.

Numerical evaluation of the quadrupole formula (§2.1) predicts a peak strain of 4.1×10^{-23} at 10 Mpc and at $f \sim 20$ Hz. The total energy released in GWs is about 2×10^{44} ergs. These results are comparable to those for AICs. However, since core-collapse supernovae are nearly 1,000 times more common than AICs, we are much more likely to detect a nearby core-collapse supernovae. To get a better handle on the potential of bar instabilities in core-collapse, we use our collapse models to construct a bar and calculate the GW emission from this bar (§2.3). We do this calculation by assuming that all of the matter up to some enclosed critical mass becomes unstable and forms a bar (conserving angular momentum), and then calculate the GW emission as a function of total unstable mass (Fig. 6). Note that strains as high as 10^{-22} are possible with frequencies as high as a kHz (Table 1). However, one should keep in mind we have assumed that *all* of the enclosed mass ends up in the bar. These estimates are relatively strong upper limits (although the strain could increase if we allowed the bar to contract and spin up). We illustrate the detectability of waves from bar instabilities in Figure 7. Each point on this plot illustrates a different possible bar, varying the amount of mass that participates in the instability. Open circles illustrate the wave strain for a single GW cycle; filled circles give the characteristic strain obtainable if the bar emits coherently for 100 cycles (see Appendix A for further

discussion). This plot demonstrates that bar modes are potentially promising sources of waves if bars remain coherent for at least a moderate (~ 50 – 100) number of GW cycles.

As the density is centrally peaked, the fragmentation instability is unlikely to occur in core-collapse supernovae. However, if it did occur, the strain would be $\sim 10^{-22}$, at frequencies as high as 2 kHz (Table 1).

4.2.2. Remnants

Core-collapse supernovae produce both neutron stars and black holes. GW emission from young neutron stars produced in core-collapse proceeds similarly to AICs. The major difference is that in core-collapse supernovae a considerable amount of fallback can occur at late times, subsequently spinning up and reheating the young neutron star. Generally, lower mass stars produce less fallback, but the fallback material accretes at a higher rate and at earlier times (Fryer et al. 1999b). We have calculated the GW emission, spin down rate, and r-mode amplitude for two fallback rates from Fryer et al. (1999b): $0.003 M_{\odot} s^{-1}$ between 20–50 s (dotted line; Fig. 4) after the launch of the explosion, and $0.0003 M_{\odot} s^{-1}$ between 2,000–9,000 s after the explosion (thick dashed line; Fig. 4). Note that fallback can cause the neutron star to spin up fast enough to emit a second burst of GWs. In all cases, the total energy emitted in GWs exceeds 10^{52} ergs, with a maximum power of over 10^{50} ergs s^{-1} . Fallback is not the only way to produce multiple bursts of gravitational waves. Numerical simulations have shown that the r-mode amplitude can grow above one and then dissipate, followed by additional growth (Lindblom, Tohline, & Vallisneri 2001). It may be difficult to tell whether a second burst is due to fallback or simply regrowth after dissipation.

As with the AICs, we stress that if the neutron star magnetic field is less than $\sim 10^{13}$ G, there will be no observational evidence of the high spin periods until late times. After a year, the GW emission will have spun the pulsar down to 11 ms, which roughly matches pulsar observations (Chernoff & Cordes, private communication). If the magnetic field is higher, these fast-spinning pulsars will affect the dynamics of the exploding material. Could this explain the polarization measurements of supernovae? If this is truly the mechanism which causes supernovae to be polarized, some supernovae should be unpolarized (e.g., the progenitor of the relatively low-field Crab pulsar).

For stars more massive than $25 M_{\odot}$ it is likely that a large amount of material will fall back onto the newly-formed neutron star, causing it to collapse to a black hole. The ringing of this newly formed black hole will produce GW emission (§2.5). In the most rapid

fallback cases, the accretion rate onto the black hole can be as high as $0.01 M_{\odot} \text{ s}^{-1}$ (Fryer et al. 1999b; MacFadyen, Woosley, & Heger 2001). For our calculations, we assumed that the black hole formed with a mass of $3 M_{\odot}$ and then accreted at a rate of $0.01 M_{\odot} \text{ s}^{-1}$ for 500 s, holding the spin fixed at $a/M_{\text{BH}} = 0.7$ for the duration of the accretion process. For an extremely optimistic estimate of the GW signal from black hole ringing, we assume that the material accretes in 0.5 s clumps ($T_{\text{thump}} = 0.5 \text{ s}$), and has a very high radiation efficiency ($\varepsilon = 0.5$). Even with such optimistic parameters, the strain for a 10 Mpc supernova turns out to be less than 5×10^{-24} and is at frequencies above 2 kHz, both too weak and outside the most sensitive band of LIGO-II. The mode mixing parameter α_{ring} has little impact on this result.

For stars more massive than $50\text{--}60 M_{\odot}$, it is likely that the star does not form a supernova at all, and instead collapses directly to a black hole. These collapsars are likely to accrete at rates as high as $1\text{--}10 M_{\odot} \text{ s}^{-1}$. For our collapsar model, we again assume the black hole forms with an initial mass of $3 M_{\odot}$ and then accretes at a rate of $1 M_{\odot} \text{ s}^{-1}$, which decreases to $0.1 M_{\odot} \text{ s}^{-1}$ after 3 s and stays constant for roughly 20 s. The black hole is assumed to start with an $a/M_{\text{BH}} = 0.5$ and spins up as it accretes to 0.7 in 1 s and then up to 0.86 in the remaining time. This model was picked to mimic the results of MacFadyen & Woosley (1999). We calculated two models, assuming the ringing is dominated by the $m = 0$ and $m = 2$ modes respectively. At $z = 1$ and using $\varepsilon = 0.5$ and $T_{\text{thump}} = 0.5 \text{ s}$, the strain can be as high as 2×10^{-23} at frequencies around 2 kHz (Fig. 8). Unfortunately, the sensitivity of LIGO type detectors is generally poor at such frequencies. Coupled with the fact that our choices for ε and T_{thump} are extremely optimistic, we believe it is extremely unlikely that the ringing waves from black holes formed in collapsars will be seen by GW detectors (Fig. 8).

5. Collapse of Very Massive Stars

At solar metallicity, stellar winds severely limit the pre-collapse mass of massive stars, and very few massive stars will remain massive up to the time of collapse. These winds are driven by the opacity of metals in the stellar envelope. It is likely that as we reduce the fraction of metals in the star, mass-loss from winds will decrease. Population III stars are the first generation of stars formed in the early universe, when virtually no metals existed (stars produce all of the metals we see today). In this section we review the death of very massive, population III stars ($100\text{--}500 M_{\odot}$). Like Chandrasekhar-massed white dwarfs, these stars must suffer one of two fates: either they explode in a giant thermonuclear explosion (“hypernova”) or they collapse to form black holes. The fate is determined by the

stellar mass. If the star’s mass exceeds $\sim 260 M_{\odot}$, it will collapse to a black hole (Fryer et al. 2001; Baraffe, Heger, & Woosley 2001). However, if the star is rotating, rotational (plus thermal) support prevents the star from undergoing immediate collapse to a black hole (Fryer et al. 2001). Rotating, very massive stars collapse and bounce, forming a much larger compact core than those produced by core-collapse supernovae: a 50–70 M_{\odot} , 1000–2000 km proto-black hole instead of the 1 M_{\odot} , 100 km proto-neutron star. This rotating proto-black hole is susceptible to bar instabilities and may produce a strong GW signal (see also Madau & Rees (2001)).

5.1. Formation Rate and Angular Momentum

Estimating an accurate rate of core-collapse from very massive stars depends on two rather uncertain quantities: the amount of matter found in population III stars and the number of these stars which actually collapse to form black holes. The mass distribution of stars at birth is known as the initial mass function (IMF). Today the IMF is peaked toward low mass stars, such that 90% of stellar core-collapse occurs in stars between 8 and $\sim 20 M_{\odot}$, and only 1% of core-collapse occurs in stars more massive than 40 M_{\odot} . However, it has long been believed that the first generation of stars after the Big Bang tended to be more massive than stars formed today (e.g., Silk 1983; Carr & Rees 1984). Recent simulations by Abel, Bryan, & Norman (2000) suggest that the typical mass of first generation stars is $\sim 100 M_{\odot}$ and it could be that a majority of Population III stars had masses in excess of 100 M_{\odot} .

The light from these very massive stars re-ionizes the early universe, and from this we can derive a constraint on the formation rate of these stars. Although we expect that these photons ionized a significant fraction of the early universe, there should not be so many stars that they ionize the universe several times over. Using our best estimates of the re-ionization fraction, the amount of ultraviolet photons produced by these massive stars, and the ionization efficiency of massive stars, one estimates that roughly 0.01% – 1% of the baryonic matter in the universe was incorporated into very massive stars (Abel et al. 2000). This corresponds to roughl $10^4 - 10^7$ very massive stars produced in a $10^{11} M_{\odot}$ galaxy, or a rate of massive stellar collapse as high as one every few thousand years

We should temper these results with two conditions. First, these stars are Population III stars, and so are born at high redshift ($z \gtrsim 5$). As they evolve to collapse in less than a few million years (Baraffe et al. 2001), they will only be observed at the high redshifts of their birth. Although we might believe our formation rate of very massive stars (within a few orders of magnitude), it is currently impossible to determine how many very massive

stars are produced with masses beyond the $\sim 260 M_{\odot}$ mass limit necessary for black hole formation. The Galaxy could produce a million of these objects, or perhaps just a few hundred. Assuming 1–10 million very massive stars per galaxy beyond $z = 5$ gives us a secure upper limit. The rotation of these stars has again been calculated using the stellar evolution code developed by Heger (1998), and for this analysis we use the Fryer et al. (2001) rotation profiles (Fig. 2).

5.2. Gravitational Waves

5.2.1. *GW from Collapse or Explosion*

The proto-black hole formed in the collapse of a massive star is expected to become secularly unstable (Fig. 1), and these secular instabilities are likely to develop before the proto-black hole collapses to a black hole (Fryer et al. 2001). With the large amount of mass ($\sim 70 M_{\odot}$) and angular momentum (Fig. 2), it is not surprising that these objects produce strong GW signals. However, the cosmological redshift moves the peak of the source waves out of the band of LIGO detectors: even at the relatively low value $z = 5$ (luminosity distance ~ 48 Gpc), the strain from bar modes peaks at frequencies less than 10 Hz, with a strain 8×10^{-23} . This is well below the LIGO II threshold. Even coherent integration over ~ 100 cycles is unlikely to produce a detectable signal; see Figs. 6 and 9.

The waves from massive star collapse may be detectable if a fragmentation instability occurs. With our crude model of fragmentation, we find that both strain and frequency are boosted if the core splits into two pieces which then fall into a Keplerian orbit, conserving angular momentum. If this instability occurs and the pieces orbit coherently for ~ 10 cycles, these waves may be detectable at redshifts $z \sim 5$; see Figs. 9 and 10.

5.2.2. *GW from Remnants*

Because the proto-black hole collapses before it can cool, the bulk viscosity prevents the growth of r-modes up to collapse. No GW radiation will occur from r-modes during the collapse of very massive stars.

After the black hole forms out of the inner $10\text{--}20 M_{\odot}$, material rapidly accretes onto it (Fig. 11). Like collapsars, this accretion rate can be very high and produce strong ringing in the newly formed black hole. Using the accretion rate and spin evolution from the simulations of Fryer et al. (2001), we estimated GW emission from $m = 0$ and $m = 2$

modes. We set the radiative efficiency parameter $\varepsilon = 0.1$ (moderately optimistic) and put $T_{\text{thump}} = 0.1$ s (indicating a relatively clumpy flow). At $z = 5$, the waves are in LIGO’s band, but do not achieve strains large enough to guarantee detection: we find that $h \sim 6 \times 10^{-23}$ initially (nearly touching the LIGO-II noise level), and that the strain rapidly decreases after that; see Fig. 8. We also illustrate these waves for a collapse at $z = 20$; they are at even lower frequency and weaker strain. This figure makes us rather pessimistic about the likelihood of measuring black hole ringing waves from the collapse of very massive stars. We note, however, that in the case $z = 5$ the accumulated signal-to-noise is of order unity.

6. Conclusion

We have examined GW production under a wide range of stellar collapse scenarios, assuming various mechanisms for GW generation. Our results indicate that some of these waves are likely to be of detectable strength, even though modern models of collapse progenitors predict less angular momentum than they did previously. The main results of our analysis are as follows.

For the accretion-induced collapse (AIC) of a white dwarf, the largest potential source of GWs during the explosion is likely to be from bar formation. However, the data used in this analysis indicate that the AIC proto-neutron star will not be unstable to bar formation, so we have not considered this mechanism. (We note, though, that Liu & Lindblom (2001) consider white dwarfs with larger angular momentum, and these would certainly be unstable to bar mode formation; further work will no doubt clarify the effectiveness of such objects for GW production.) The newly formed remnant is hot enough that it should be unstable to the production of r-mode GWs. The event rate for AICs is fairly low ($\sim 10^{-5}$ yr $^{-1}$ per galaxy), so one must consider events as far out as 100 Mpc. At this distance, both r-mode and bar-mode (if they occur) waves are unlikely to be detectable.

For core-collapse supernovae, a bar-mode instability is likely to develop shortly after the launch of the supernova shock, similar to the case of AICs. Core-collapse supernovae are much more frequent than AICs ($\sim 10^{-2}$ yr $^{-1}$ per galaxy), so we do not have to look quite so far out; we consider collapse out to about 10 Mpc. For a range of bar formation scenarios, we find frequencies and strains that fall above the LIGO-II noise curve. High signal-to-noise measurements are possible if the bar remains coherent for tens to hundreds of cycles. The collapse forms a rapidly spinning neutron star, which may be unstable to r-mode emission. The r-modes can form in the hot remnant itself, or be “reactivated” somewhat later when hot material falls back onto the star, reheating it and increasing its spin. These waves should be detectable by LIGO-II. Very massive progenitors form a black

hole instead of a neutron star. This case produces no r-mode emission, but there will be GWs from ringing of the black hole horizon. However, even with ridiculously optimistic assumptions about the nature of the matter flow onto the hole, we find that these waves are completely undetectable — their strains are very weak, and they are emitted at high frequencies ($f \sim 2000\text{--}5000$ Hz) where detectors have poor sensitivity.

We also consider the collapse of $300 M_{\odot}$ stars as a source of GW emission. Although these massive stars may have been quite common in the first generation of stars, it is unlikely that they formed at redshifts below five. When very massive stars collapse, they pass through a phase where the matter is densely clumped into a proto-black hole. This rapidly rotating object is susceptible to bar mode instabilities, producing a fairly large GW strain. However, the GWs are unlikely to be detectable because of the large frequency shift due to the cosmological redshift and we find that bar formation at redshift $z \sim 5$ is marginally detectable only if the bar persists for hundreds of cycles. If the proto-black hole material were to fragment into clumps (which we model as a binary), it could yield a signal detectable by LIGO-II. As the proto-black hole remains extremely hot until collapse, the bulk viscosity prevents an r-mode instability from developing. Although we believe it is unlikely, it is possible that the ringing of the newly born black hole *might* be detectable. We find that if the star collapses at $z \sim 5$, the ringing waves are emitted at high enough frequency ($f \sim 30\text{--}50$ Hz) that detector noise may not overwhelm the signal. If the collapse is asymmetric and “clumpy” enough to severely distort the hole for several seconds, the ringing waves are likely to be of interesting strength. We hope that this result will motivate more careful analyses of ringing waves from BHs that are produced in massive stellar collapse (an example of which is described in Papadopoulos & Font (2001)). It is also to be noted that Madau & Rees (2001) have recently examined massive black holes as remnants from population III stars. In their paper they mention the emission of GWs from the capture of such holes onto supermassive black holes at the centers of galaxies. Such waves are very different from those discussed here, and in fact would be sources for low-frequency space-based detectors such as LISA. We have not considered this mechanism here.

For all of our estimates we have made a number of assumptions, chosen to ensure a safe maximum of the gravitational wave signal. Therefore all of our results should be taken as upper limits, and it is certainly possible that the GW signals are weaker than our calculations suggest. In addition, although based on recent collapse calculations, any estimate of the gravitational wave signal will be limited by the uncertainties in the core-collapse models. However, it is unlikely that our upper limits will change significantly as collapse simulations improve.

C.L.F. gratefully acknowledges the support of the Institute for Theoretical Physics

where this work was initiated. The authors are grateful to Luciano Rezzolla and John Beacom for useful comments, to David Shoemaker and Kip Thorne for pointing out some errors, and to Warner Miller for interesting discussions in the course of this work. The work of C.L.F was funded by the ITP visitor program and a Feynman Fellowship (LANL). D.E.H and S.A.H. are supported by NSF Grant PHY-9907949 at the ITP.

A. Detectability criteria

Because of the weakness of GWs, sophisticated data processing methods are needed to pull astrophysical signals from a detector’s noisy data stream. Here we discuss some useful figures of merit that characterize the effectiveness of such techniques. We use these results to describe how well the GW strains discussed in this paper can be detected by GW detectors, focusing in particular on the second generation LIGO interferometers (“LIGO-II”).

One statistic in particular is of great importance to us: the signal power ρ^2 , given by

$$\rho^2 = 4 \int_0^\infty df \frac{|\tilde{h}(f)|^2}{S_h(f)}, \quad (\text{A1})$$

where $\tilde{h}(f)$ is the Fourier transform of the gravitational waveform $h(t)$, and $S_h(f)$ is the spectral density of strain noise.

One of the most important methods of searching for GWs is called “matched filtering”. This method uses a model or template for the waveform to construct a linear filter. The instrumental data are then correlated with the filter, yielding a signal-to-noise ratio (SNR). If a signal in the data stream matches the template, then the SNR has a mean value ρ :

$$\left(\frac{S}{N}\right)_{\text{MF}} = \rho. \quad (\text{A2})$$

The signal power is often referred to as the matched filtering SNR. It is simple to prove that this SNR is the maximum obtainable with linear filters, so this technique is sometimes called “optimal filtering”. Signals are detectable if the matched filtering SNR exceeds a threshold, ρ_{thresh} , whose value depends on a large number of parameters (number of templates in the filter bank, duration of the templates, number of detectors, etc.). As a rough rule of thumb, $\rho_{\text{thresh}} \simeq 5$. Further discussion of this point can be found in Flanagan & Hughes (1998), particularly the text near Eqs. (2.8) and (2.9).

Because the GWs from a particular source depend upon the source’s position on the sky, and its orientation, the SNR should be averaged over these quantities. Flanagan &

Hughes (1998) have shown that the matched filtering SNR, so averaged, depends only on the spectrum of GW energy dE/df :

$$\langle \rho^2 \rangle = \frac{2(1+z)^2}{5\pi^2 D(z)^2} \int_0^\infty df \frac{1}{f^2 S_h(f)} \frac{dE}{df} [(1+z)f], \quad (\text{A3})$$

where z is the cosmological redshift of the source, and $D(z)$ is its luminosity distance.

The matched filtering SNR formula can be rewritten as follows:

$$\langle \rho^2 \rangle = \int_0^\infty \frac{df}{f} \left[\frac{h_{\text{char}}(f)}{h_{\text{noise}}(f)} \right]^2. \quad (\text{A4})$$

Using Eq. (A3) as our model, the “characteristic signal strain” $h_{\text{char}}(f)$ is given by

$$h_{\text{char}}(f) = \frac{\sqrt{2}(1+z)}{\pi D(z)} \sqrt{\frac{dE}{df} [(1+z)f]}. \quad (\text{A5})$$

Note that if one knows the characteristic strain for a single cycle, the value for N cycles is just

$$h_{\text{char}} \simeq \sqrt{N} h_{\text{char}, 1 \text{ cycle}} \quad (\text{A6})$$

since dE/df accumulates with the number of cycles. (The equality is exact if the signal is monochromatic.) The “mean noise strain” $h_{\text{noise}}(f)$ is

$$h_{\text{noise}}(f) = \sqrt{5f S_h(f)}. \quad (\text{A7})$$

The factor of $\sqrt{5}$ in this equation arises from the detector’s sensitivity pattern, which effectively increases the noise for sky averaged sources. Note that the noise spectral density $S_h(f)$ used in Eq. (A7) is the square of the quantity plotted in Gustafson et al (1999). The strains $h_{\text{char}}(f)$ and $h_{\text{noise}}(f)$ indicate in a simple way the relative strength of the astrophysical GW signal and the noise at a particular frequency. Comparing them is an effective way of quickly estimating the signal power: if $h_{\text{char}}(f) > h_{\text{noise}}(f)$, then the signal is likely to be detectable with matched filtering, and hence worth further analysis. In Figs. 5 and 7–9 we show $h_{\text{char}}(f)$ for the various GW emission scenarios discussed in this paper.

Throughout this paper we use the broad-band LIGO-II noise curve described in Gustafson et al. (1999). In particular, it is used to compute $h_{\text{noise}}(f)$ as plotted in the figures. LIGO-II is a planned upgrade to the detectors at the two LIGO sites. Research and development for various LIGO-II components is in progress, with final implementation set to begin in 2006 or shortly thereafter. One of LIGO-II’s design goals is to have a moderately

tunable sensitivity profile; the broad-band curve we use here is a useful configuration for analyzing the detectability of sources that are not very well understood. Other possible configurations include a curve optimized for detecting binary neutron stars, and a curve with moderately narrow band sensitivity. See Gustafson et al. (1999) for further discussion and details.

A second statistic that could easily be computed (though we do not do so here) is the time-frequency volume \mathcal{N} :

$$\mathcal{N} = 2T\Delta f . \tag{A8}$$

The quantity T is a duration and Δf a bandwidth. For the purpose of estimating the detectability of astrophysical signals, T is the duration of the signal and Δf its frequency bandwidth. (In an actual GW search, T and Δf may be treated as variational parameters so that events are not missed.)

This statistic is useful because it helps to understand how well techniques that are not based on matched filtering might perform. A large value of \mathcal{N} indicates that the signal power is “smeared” over a wide range of frequencies or Fourier bins, and that a signal may be difficult to reconstruct without a great deal of prior information. For example, suppose we know that the signal has support only in some bandwidth $\Delta f = f_{\text{high}} - f_{\text{low}}$. Rather than using a matched filter (which we do not have enough information to construct), data analysis would use a simple band-pass filter. This filter chops out all power in the datastream at frequencies above f_{high} and below f_{low} . The SNR obtained with this filter is the ratio of the signal peak amplitude to the noise peak amplitude in the filtered datastream. Following the analysis of Flanagan & Hughes (1998), this is given by

$$\left(\frac{S}{N}\right)_{\text{BPF}} \simeq \frac{\rho}{\sqrt{\mathcal{N}}} . \tag{A9}$$

A useful rule of thumb is that signals are detectable with band-pass filtering if $(S/N)_{\text{BPF}} \geq 1$.

The band-pass filtering SNR is a kind of worst case scenario, applicable when very little is known about the signal’s characteristics. The matched filtering SNR is a best case scenario, for when the signal is very well understood. A more middle-of-the-road diagnostic is the excess power statistic, first introduced in Flanagan & Hughes (1998), and discussed at length in Anderson et al. (2001). This search technique requires knowledge of the duration T and frequency bandwidth Δf . It works by dividing the frequency domain data into bins of width $\delta f \sim 1/T$ and incoherently combining the power in each bin. The resultant statistic, \mathcal{E} , is a measure of the total energy in the datastream. Detection of a signal occurs when the value \mathcal{E} exceeds what would be expected from noise alone in a statistically

significant way. The analysis of Anderson et al. (2001) tells us that this occurs when

$$\rho^2 > \sqrt{2\mathcal{N}}. \quad (\text{A10})$$

We thus have some useful rules of thumb for estimating the detectability of a GW signal. First, calculate the sky-averaged SNR, Eq. (A3), and the time frequency volume, $\mathcal{N} = 2T\Delta f$. If $\langle \rho^2 \rangle^{1/2} \equiv \rho_{\text{ave}}$ is of order 5 or so, then this is a potentially interesting source. If ρ_{ave} is closer to unity, then it will be hard to detect, but probably should not be dismissed out of hand. On the other hand, if ρ_{ave} is much less than unity there is little chance the signal will be detected.

If ρ_{ave} indicates that the source is interestingly strong, examine $\rho_{\text{ave}}/\sqrt{\mathcal{N}}$, the band-pass filtering SNR. If this is of order 1 or greater, then the source should be detectable without too much sophisticated data analysis. If ρ_{ave} is large but $\rho_{\text{ave}}/\sqrt{\mathcal{N}}$ is small, then some detailed knowledge of the source’s characteristics will be needed to aid data analysis. A good idea of how much detail is needed can be obtained by checking the number $\rho_{\text{ave}}/\mathcal{N}^{1/4}$. If this measure is large, then the excess power statistic is likely to be useful. In this case, just knowing the signal’s likely bandwidth and duration should be enough to significantly aid data analysis.

Table 1. Gravitational Wave Emission

Object	Emission Mechanism	Rate ^a (yr ⁻¹)	Typical Distance	h(f) (10 ⁻²⁴)	f(Hz)	Max. Power ergs s ⁻¹
AIC ^b	Numerical ^c	$\lesssim 10^{-5}$	100 Mpc	5.9	~ 50	10^{48}
	r-modes ^c			0.35	~ 1000	10^{50}
SN ^b	Numerical ^c	$\lesssim 10^{-2}$	10 Mpc	41	~ 20	10^{45}
	Bar-modes ^c			100	~ 1000	10^{53}
	Binary ^c			100	~ 2000	10^{54}
	r-modes ^c			0.35	~ 1000	10^{50}
	BH Ringing ^c			5, 2	$\sim 2000, \sim 2000$	10^{55}
300M _⊙ ^b	Numerical ^c	$\lesssim 10^7$	z=5, z=20	80, 20	$\lesssim 2 - 10, \lesssim 0.5 - 2.5$	10^{42}
	Bar-modes ^c			7, 5	~ 10	10^{54}
	Binary ^c			120, 80	~ 30	10^{56}
	BH Ringing ^c			60, 30	$< 70, < 20$	10^{57}

^aFor AICs and Supernovae, we have given the rate in number per year for a Milky-Way massed galaxy. The number given for the collapse of 300M_⊙ stars is the rate in the universe per year (assuming upper limits on the rate and roughly 10¹⁰ Milky-Way massed galaxies in the universe). Although this number is extremely high, remember that only those that occur at low redshifts will even rise above the sensitivity curve of LIGO-II. In addition, the rate is only an upper limit of an extremely uncertain number which may be many orders of magnitude lower.

^bAIC ≡ accretion-induced collapse (see §3); SN ≡ core-collapse supernovae (see §4), note that there are two values for BH ringing, the former for fallback, and the latter for collapsars; 300M_⊙ ≡ 300 M_⊙ population III stars (see §5), note that we consider two values for 300 M_⊙ stars, the former for systems at z = 5, the latter for z = 20.

^cNumerical ≡ Numerical Quadrupole Method (see §2.1), Bar-modes (see §2.2), Binary (see §2.3), r-modes (see §2.4), BH ringing (see §2.5).

REFERENCES

- Abel, T., Bryan, G. L., & Norman, M. L. 2000, *ApJ*, 540, 39
- Andersson, N. 1998, *ApJ*, 502, 708
- Anderson, W. G., Brady, P. R., Creighton, J. D. E., & Flanagan, E. E. 2001, *Phys. Rev. D* 63, 042003 (2001); also gr-qc/0008066.
- Ando, M. and Tsubono, T., in “Gravitational Waves: Proceedings of the 3rd Edoardo Amaldi Conference”, edited by S. Meshkov (AIP Conference Proceedings 523, Melville, New York, 2000), p. 128
- Baade, W., & Zwicky, F. 1934, *Phys. Rev.*, 45, 138
- Bahcall, N., Ostriker, J. P., Perlmutter, S., & Steinhardt, P. 1999, *Science*, 284, 1481
- Baraffe, I., Heger, A., & Woosley, S.E. 2001, *ApJ* in press, astro-ph/0009410
- Blanchet, L., Damour, T., Schäfer, G. 1990, *MNRAS*, 242, 289
- Branch, D. 1998, *ARA&A*, 36, 17
- Brown, D. 2001, in the proceedings of the workshop on “Astrophysical Sources for Ground-Based Gravitational Wave Detectors” at Drexel University, Philadelphia, ed. Joan Centrella, AIP, gr-qc/0012084
- Cappellaro, E., Turatto, M., Tsvetkov, D. Yu., Bartunov, O.S., Pollas, C., Evans, R., Hamuy, M. 1997, *A&A*, 322, 431
- Cassisi, S., Iben, I., Jr., & Tornambé, A. 1998, *ApJ*, 496, 376
- Centrella, J.M., New, K.C.B., Lowe, L.L., & Brown, J.D. 2000, *submitted to ApJ*, astro-ph/0010574
- Chandrasekhar, S. 1969, *Ellipsoidal Figures of Equilibrium* (Yale University Press, New Haven).
- Chandrasekhar, S. 1983, *The Mathematical Theory of Black Holes* (Oxford University Press, New York). Note that Chandrasekhar uses the opposite sign on m , so that his strongly suppressed mode is $m = 2$.
- Colgate, S.A., & White, R.H. 1966, *ApJ*, 143, 626
- Davis, M., Ruffini, R., Press, W. H. & Price, R. H., 1971, *Phys. Rev. Lett.*, 27, 1466

- Echeverria, F. 1989, Phys. Rev. D, 40, 3194
- Flanagan, E. E., & Hughes, S. A. 1998, Phys. Rev. D 57, 4535
- Friedman, J. L., & Morsink, S. M. 1998, ApJ, 502, 714
- Fryer, C.L., Benz, W., Colgate, S.A., Herant, M., 1999a, ApJ, 516, 892
- Fryer, C.L., Colgate, S.A. & Pinto, P.A., 1999b, ApJ, 511, 885
- Fryer, C.L. & Heger, A., 2000, ApJ, 541, 1033
- Fryer, C.L., & Kalogera, V. 2001, accepted by ApJ
- Fryer, C.L., Woosley, S.E., & Heger, A., 2001, accepted by ApJ
- Gustafson, E., Shoemaker, D., Strain, K., Weiss, R. 1999 LSC White Paper on Detector Research and Development, LIGO Document T990080-00-D.
- Heger, A. 1998, Ph.D. thesis, Technische Univ. München
- Hillebrandt, W., Wolff, R.G., Nomoto, K. 1984, ApJ, 133, 175
- Ho, W. C. G., Lai, D. 2000, ApJ, 543, 386
- Hogg, D. W. astro-ph/9905116.
- Isaacson, R. A. 1968, Phys. Rev., 166, 1272
- Kato, M. & Hachisu, I. 1999, ApJ, 513, L41
- Keil, W., & Janka, H.-T. 1995, A&A, 296, 145
- King, A. R., & Lasota, J.-P. 1991, ApJ, 378, 674
- King, A. R., Wynn, G. A., Regev, O. 1991, MNRAS, 251, 30
- Kuroda, K. et al., Int. J. Mod. Phys. D, 8, 557 (2000)
- Leaver, E. W., 1985, Proc. R. Soc. Lond., A402, 285
- Liebert, J. 1980, ARA&A, 18, 363
- Lindblom, L., 2001, To appear in "Gravitational Waves: A Challenge to Theoretical Astrophysics," edited by V. Ferrari, J.C. Miller, and L. Rezzolla (ICTP, Lecture Notes Series), astro-ph/0101136

- Lindblom, L., Tohline, J.E., & Vallisneri, M. 2001, PRL, 86, 1152
- Liu, Y. T., & Lindblom, L. 2001, submitted to MNRAS, astro-ph/0012198
- Livio, M. 2000, to appear in “Cosmic Explosions!”, the 10th Annual October Astrophysics Conference in Maryland, Eds. S. Holt & W.W. Zhang (1999), AIP.
- Lück, H. et al., in “Gravitational Waves: Proceedings of the 3rd Edoardo Amaldi Conference”, edited by S. Meshkov (AIP Conference Proceedings 523, Melville, New York, 2000), p. 119
- MacFadyen, A., Woosley, S.E., & Heger, A. 2001, submitted to ApJ, astro-ph/9910034
- Madau, P., & Rees, M. 2001, ApJ, 551, L27
- Marion, F. in “Gravitational Waves: Proceedings of the 3rd Edoardo Amaldi Conference”, edited by S. Meshkov (AIP Conference Proceedings 523, Melville, New York, 2000), p. 110
- McClelland, D. E. et al., in “Gravitational Waves: Proceedings of the 3rd Edoardo Amaldi Conference”, edited by S. Meshkov (AIP Conference Proceedings 523, Melville, New York, 2000), p. 140
- Narayan, R., Popham, R. 1989, ApJ, 346, L25
- Nomoto, K., Kondo, Y. 1991, ApJ, 367, L19
- Nomoto, K., Iwamoto, K., & Kishimoto, N. 1997, Science, 276, 1378
- Owen, B. J., Lindblom, L., Cutler, C., Schutz, B. F., Vecchio, A., & Andersson, N. 1998, Phys. Rev. D, 58, 084020
- Papadopoulos, P. & Font, J. A., 2001, Phys. Rev.D, in press; gr-qc/0009024.
- Rampp, M., Müller, E., & Ruffert, M. 1998, A&A, 332, 969
- Rezzolla, L, Lamb, F.K., & Shapiro, S.L. 2000, ApJ, 531, L139
- Sasaki, M. & Nakamura, T. 1982, Prog. Theor. Phys. 67, 1788.
- Teukolsky, S.A. 1973, ApJ, 185, 635
- Tohline, J., & Hachisu, I. 1990, ApJ, 361, 394
- Thorne, K.S. 1980, Rev. Mod. Phys., 52, 299

- Thorne, K.S., Price, R.H., and MacDonald, D.A. 1986, *Black Holes: The Membrane Paradigm*, Yale University Press (New Haven).
- Thorne, K.S. 1987, in *Three hundred years of gravitation*, eds. Hawking, S., and Israel, W. Cambridge University Press (Cambridge).
- Van Putten, M. H. P. M. to appear in the Proceedings of the 2001 Apsen Winter Conference on Gravitational Waves; astro-ph/0102043.
- Van Putten, M. H. P. M. and Sarkar, A. 2000, Phys. Rev. D 62, 041502.
- Woosley, S.E. & Baron, E. 1992, ApJ, 391, 228
- Woosley, S.E. 1993, ApJ, 405, 273
- Zwergner, T. & Müller, E. 1997, A&A, 320, 209

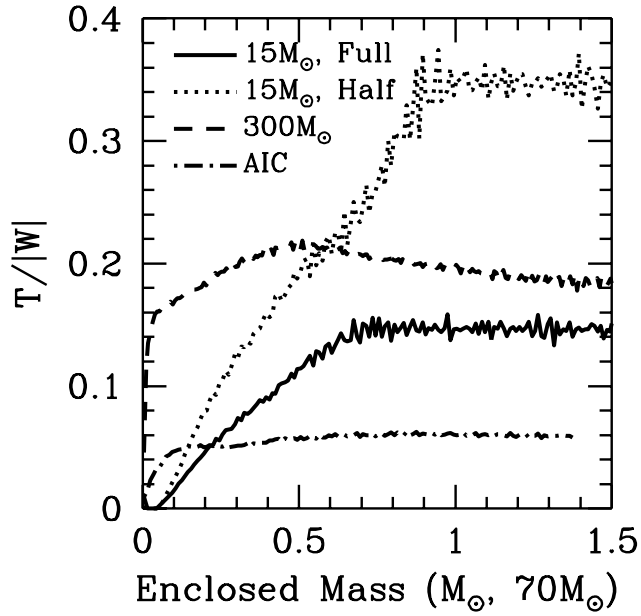


Fig. 1.— Rotational energy divided by gravitational energy ($T/|W|$) versus mass for collapsing stars. AIC, 0.18 s after collapse; rotating core-collapse (full rotation), 1.6 s after bounce; core-collapse (half rotation), 1.4 s after bounce; $300 M_{\odot}$ direct collapse, 1.9 s after collapse. For the core-collapse stars, $T/|W|$ is actually higher for the star initially spinning at half the rotation rate, as the system is more compact.

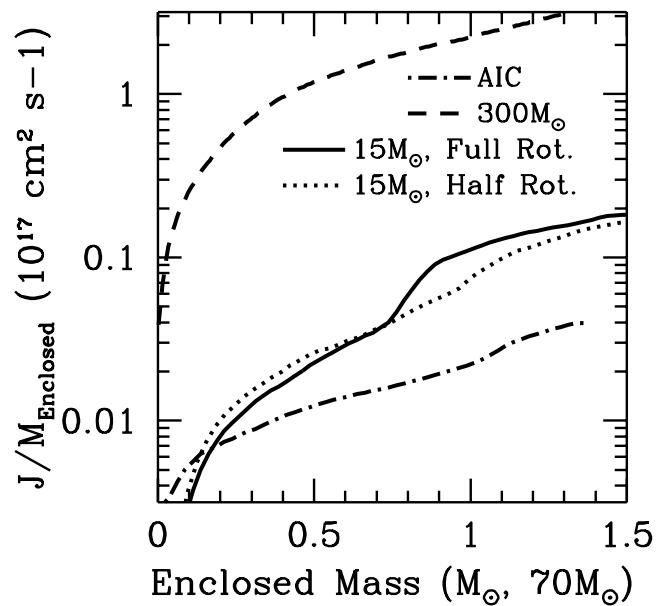


Fig. 2.— Specific angular momentum versus mass for collapsing stars. AIC, 0.18 s after collapse; rotating core-collapse (full rotation), 1.6 s after bounce; core-collapse (half rotation), 1.4 s after bounce; $300M_{\odot}$ direct collapse, 1.9 s after collapse. The $300M_{\odot}$ has, by far, the highest angular momentum.

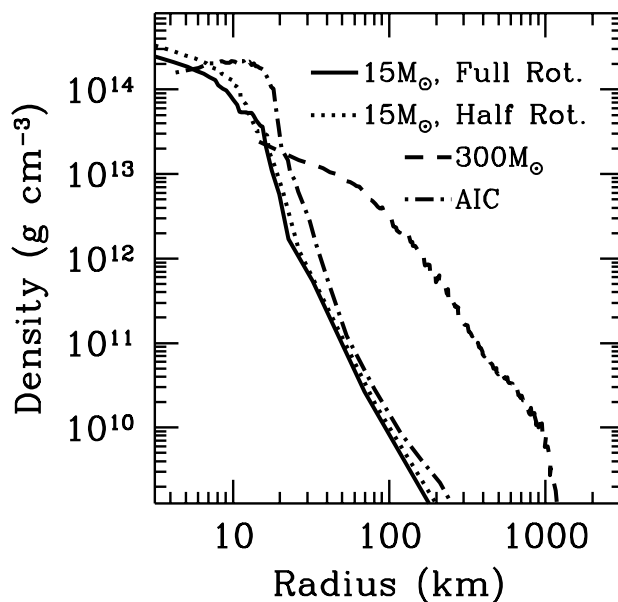


Fig. 3.— Density versus radius for collapsing stars. AIC, 0.18 s after collapse; rotating core-collapse (full rotation), 1.6 s after bounce; core-collapse (half rotation), 1.4 s after bounce; $300 M_{\odot}$ direct collapse, 1.9 s after collapse. For the core-collapse simulations, the slower rotator is more dense. Although the maximum density of the $300 M_{\odot}$ direct collapse is much lower than the other core-collapses, its mass out to 1000 km is 50 times that of the other collapsed objects.

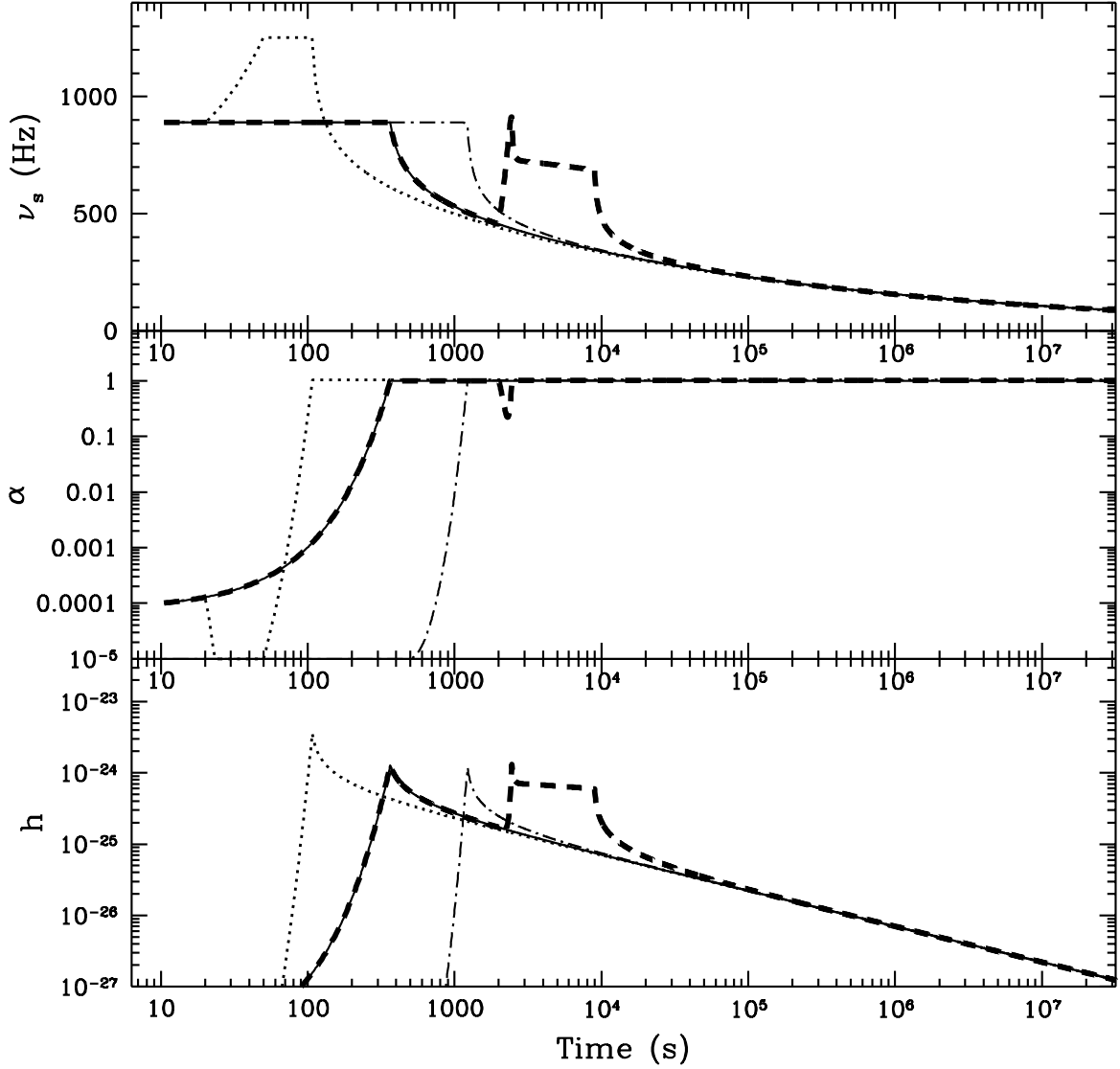


Fig. 4.— Evolution of the neutron star spin frequency (ν_s), r-mode amplitude (α), and strain (h) at 10 Mpc as a function of time. The thin solid line corresponds to a simulation assuming no fallback accretion, with the temperature of the neutron star T_9 decaying as $(t/1 \text{ yr})^{-1/6}$. The thin dot-dashed line corresponds to a temperature decaying as $(t/1 \text{ yr})^{-1/3}$. In core-collapse supernovae it is likely that some fallback will occur, and the dot-dashed line and thick dashed line correspond to an accretion rate of $0.01 M_\odot \text{ s}^{-1}$ 20 s after the explosion and $0.001 M_\odot \text{ s}^{-1}$ 2000 s after the explosion, respectively. Note that in late-time accretion the fallback material heats up the neutron star, causing the viscosity to rise and initially damp the r-mode oscillations.

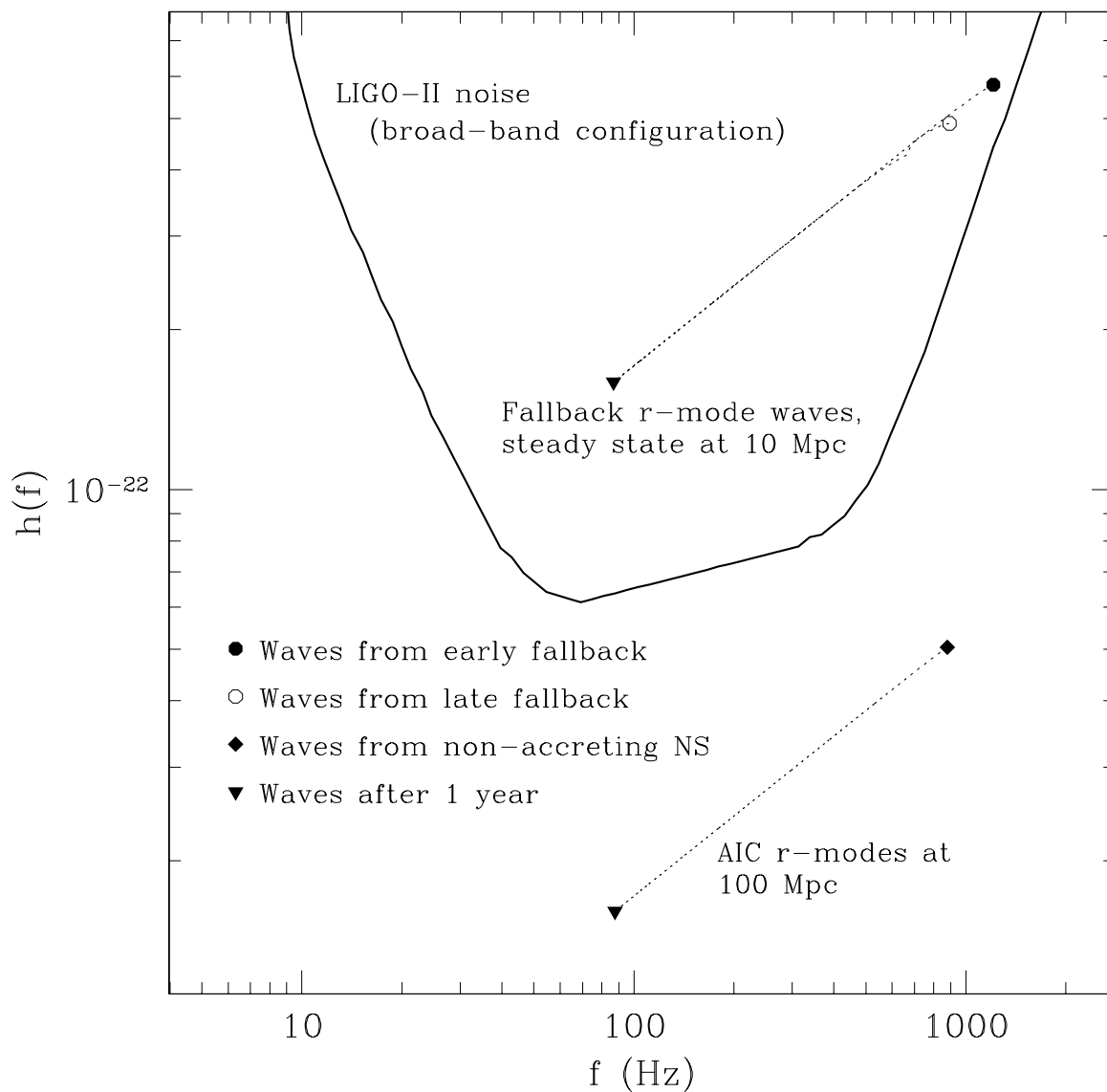


Fig. 5.— Comparison of the characteristic strains associated with r-modes to the mean noise in enhanced LIGO interferometers. The top track shows the waves emitted after early and late fallback reheats and spins up a newly born neutron star. The lower track gives the same information but for a neutron star created in accretion induced collapse. We show the AIC waves at 100 Mpc since such events are probably about 1000 times rarer than core-collapse supernovae.

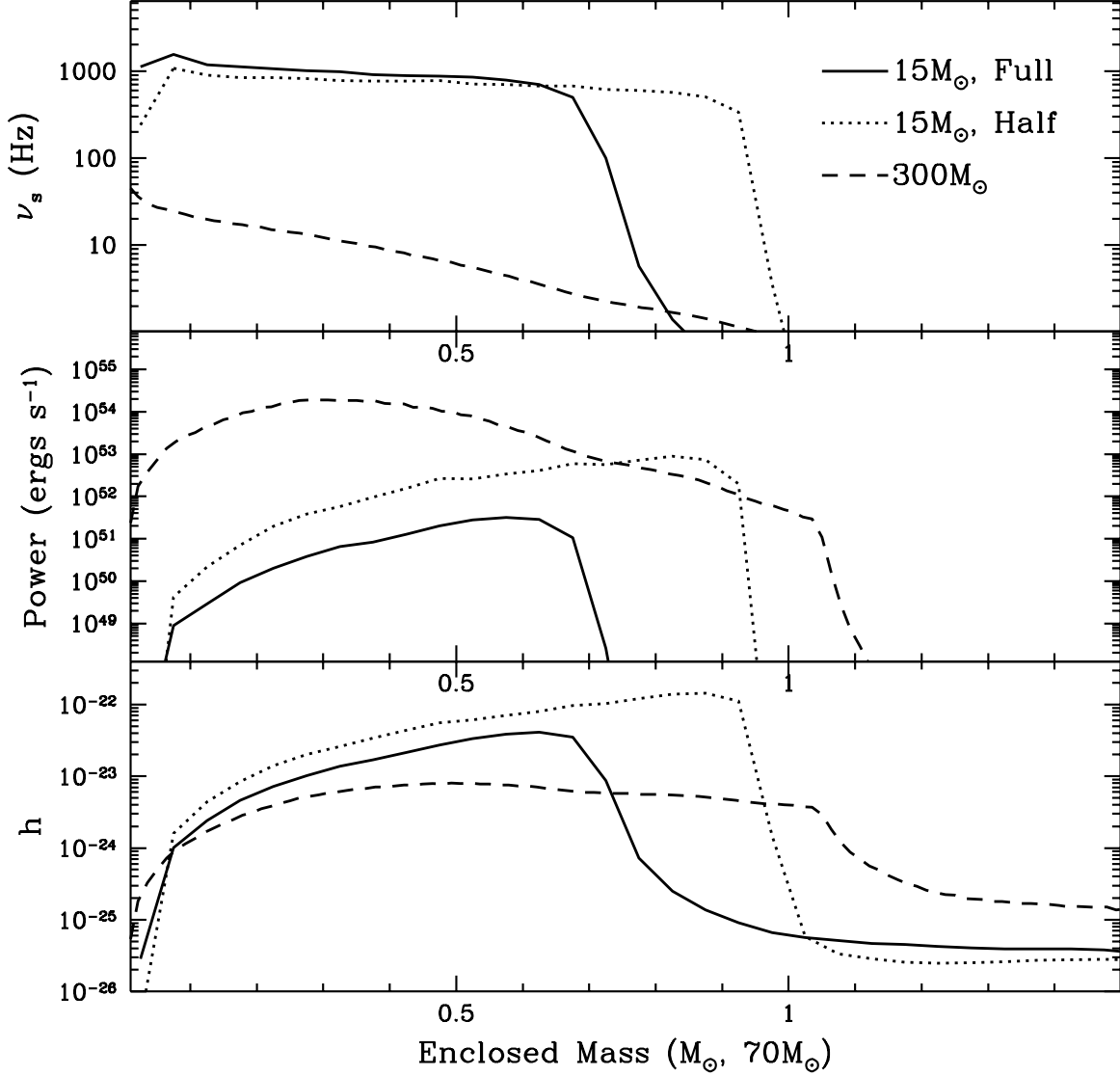


Fig. 6.— Bar-mode spin period, power, and strain versus the mass encompassed by the bar-mode instability. The proto-neutron star masses for the core-collapse models are in the range $0.8\text{--}1.0 M_\odot$, and the bar-modes are limited to within this mass regime. For the $300 M_\odot$ case, the bar modes must develop within $70\text{--}90 M_\odot$. The strain is calculated assuming a distance of 10 Mpc for the $15 M_\odot$ collapse simulations, and $z = 10$ for the $300 M_\odot$ simulations.

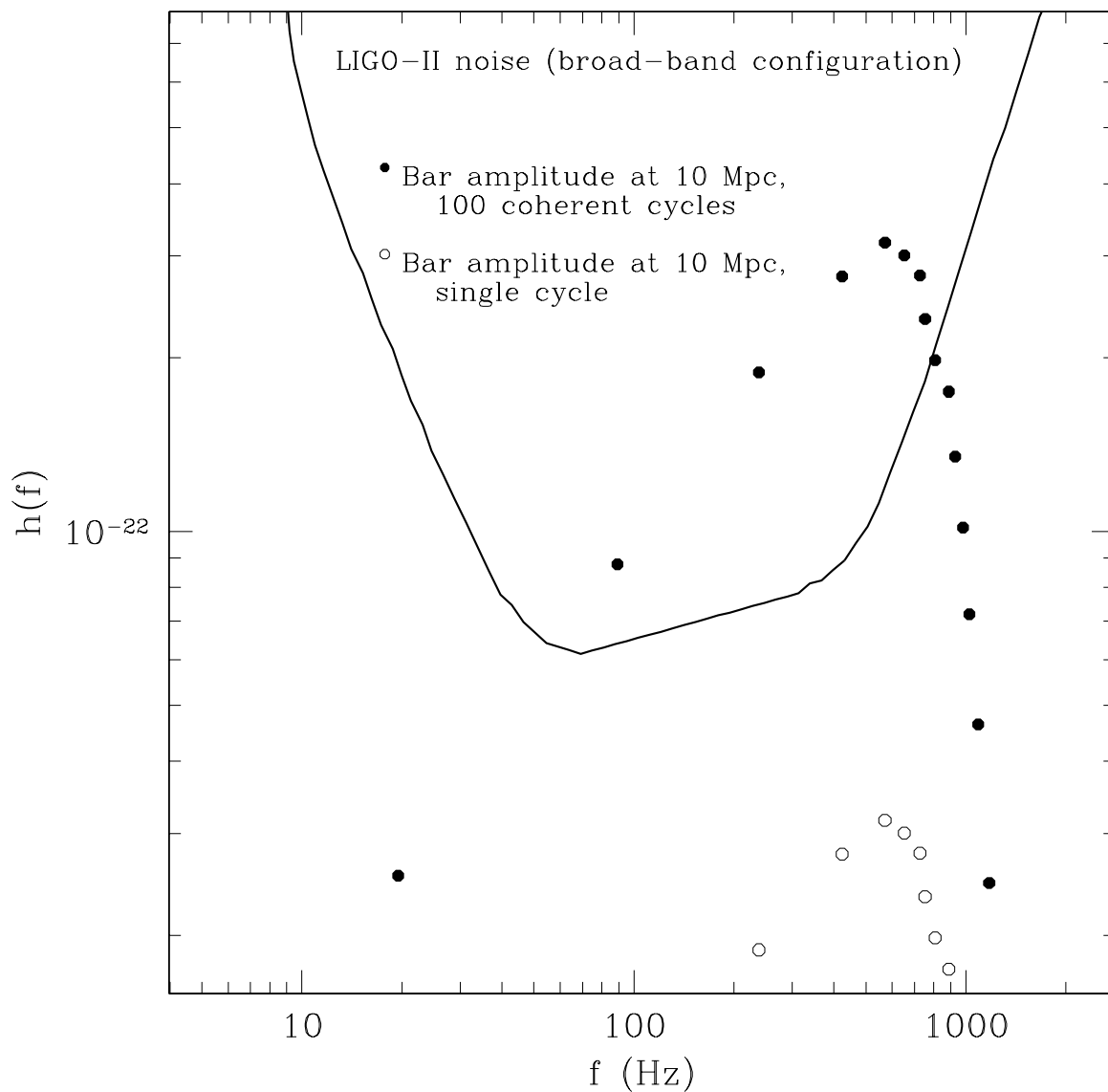


Fig. 7.— A range of possible bar mode waves emitted in the collapse of a $15 M_{\odot}$ star. We assume that all mass inside a given radius participates in the instability and forms a bar, conserving angular momentum as it forms. Each point represents the waves given off from a particular choice of radius, moving to larger radii from right to left. An open circle is the strain from a single rotation cycle of the bar; a closed circle is the integrated strain that would be measured if the bar were to remain coherent for 100 GW cycles. The range between the open and closed circles suggests that bar mode waves could be of interesting strength provided they remain coherent for a minimum of ~ 50 –100 cycles.

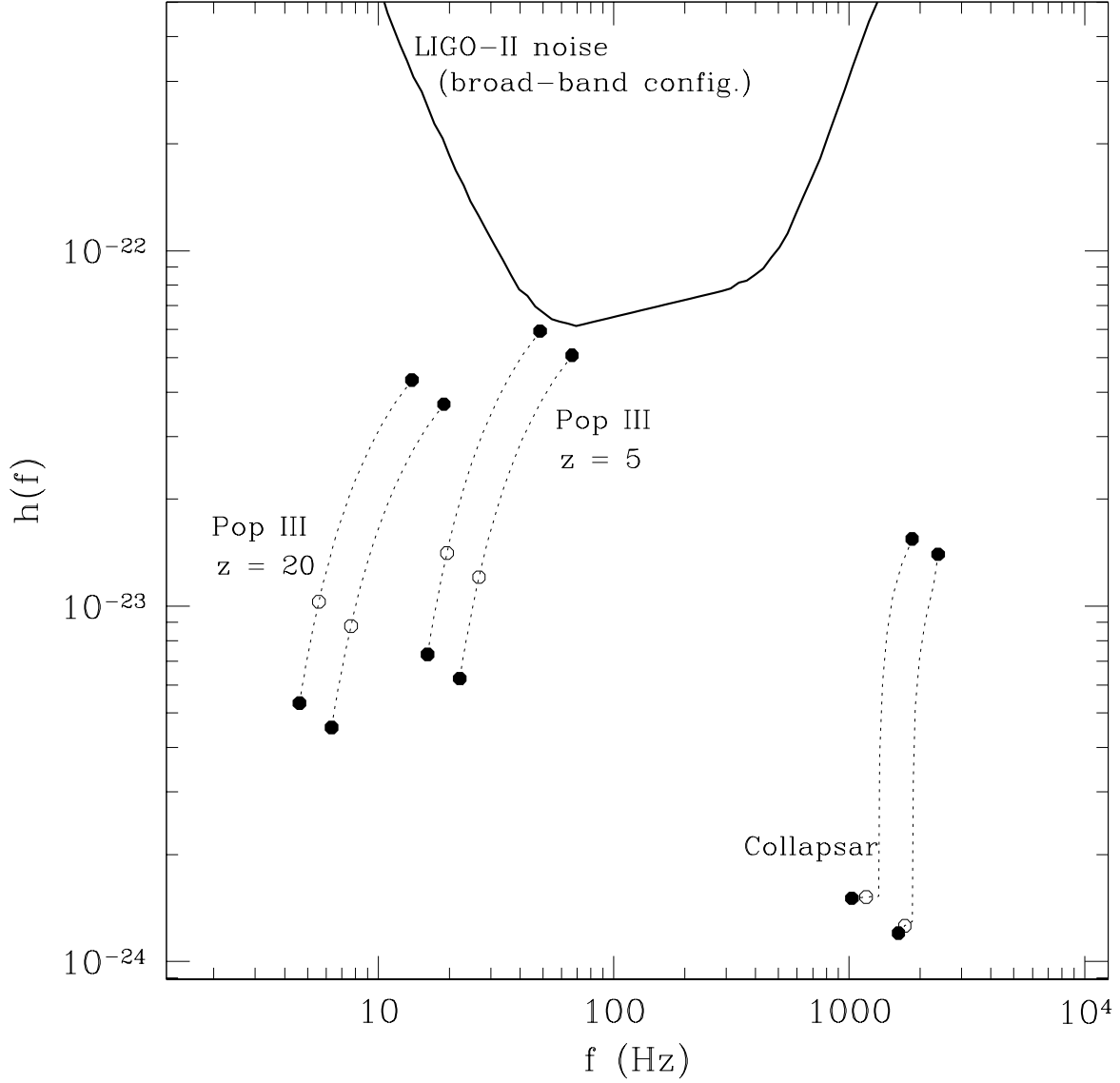


Fig. 8.— Comparison of the characteristic wavetrain for black hole ringing to the mean noise in enhanced LIGO interferometers (broad-band configuration). The two tracks for each source show the change in strain as the parameter α_{ring} [which apportions signal power between $m = 0$ and $m = 2$ modes; cf. Eq. (31)] varies from 0 to 1. The tracks begin at the upper right dark circles and evolve downwards and to the left. The open circles indicate the half way point in time of the evolution. Notice that the wavetrain associated with collapsars quickly falls to its minimum value; this is because the accretion starts out strong but is quickly reduced. The Population III waves are computed assuming the energy emission parameter $\varepsilon = 0.1$ [an optimistic choice, but not excessively so; cf. Eq. (26)] and $T_{\text{thump}} = 0.1$ seconds (indicating a fairly clumpy flow). The collapsar track assumes that $\varepsilon = 0.5$ (an extremely optimistic choice) and $T_{\text{thump}} = 0.5$ seconds (indicating a very clumpy flow).

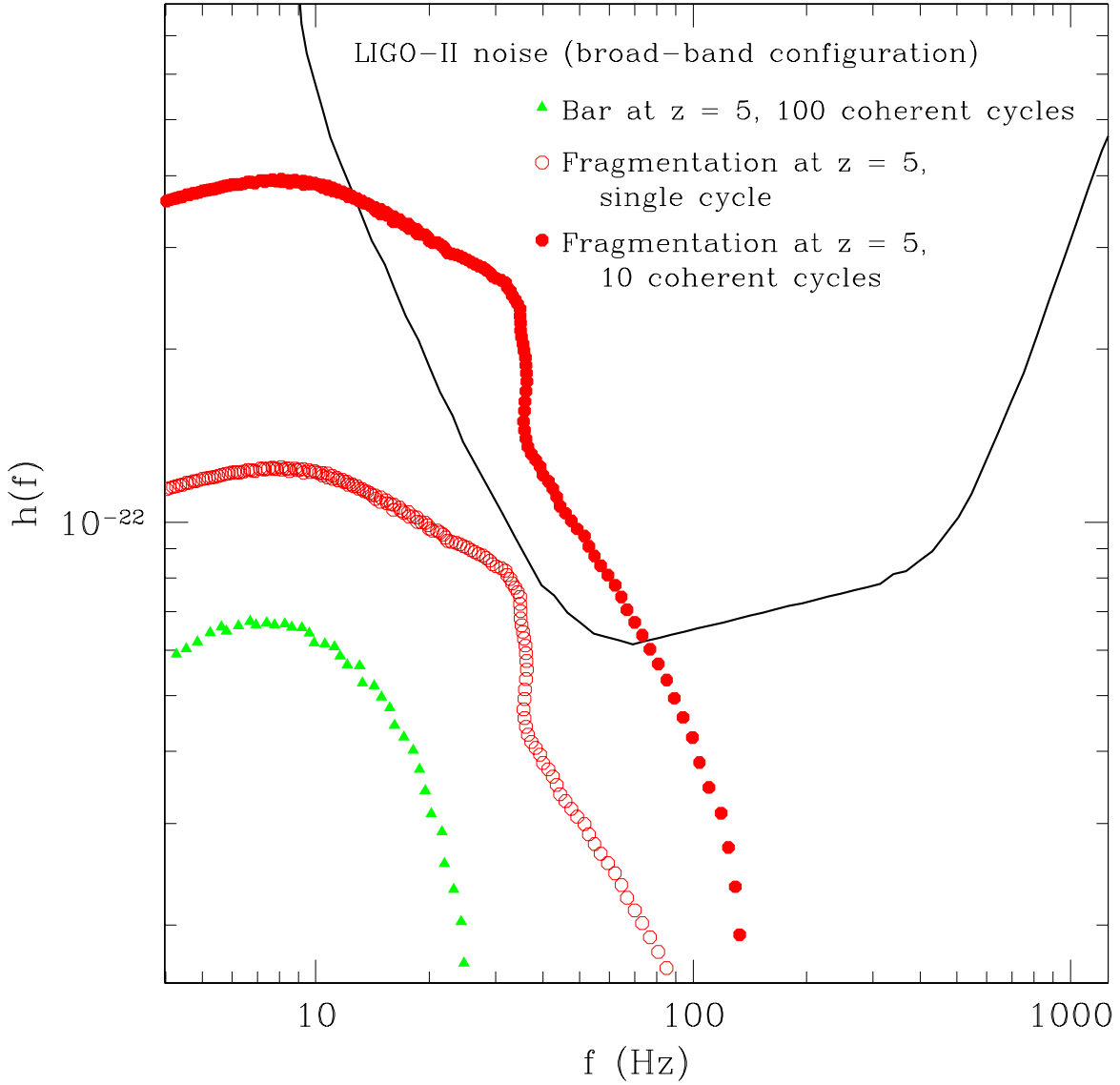


Fig. 9.— A range of possible bar mode waves emitted in the collapse of a $300 M_{\odot}$ star. Each point is calculated in the same manner as the points given in Fig. 7. The prospects for detecting bar mode waves are quite poor: the cosmological redshift slides the emission frequency out of the LIGO band. Even coherent integration for 100 cycles is insufficient for good detection prospects. The waves emitted from a fragmentation instability are more interesting: their strains and frequencies are quite a bit higher, and may be accessible to LIGO. If the waves from such a fragmentation were to remain coherent for some number of cycles, they could make an interesting source.

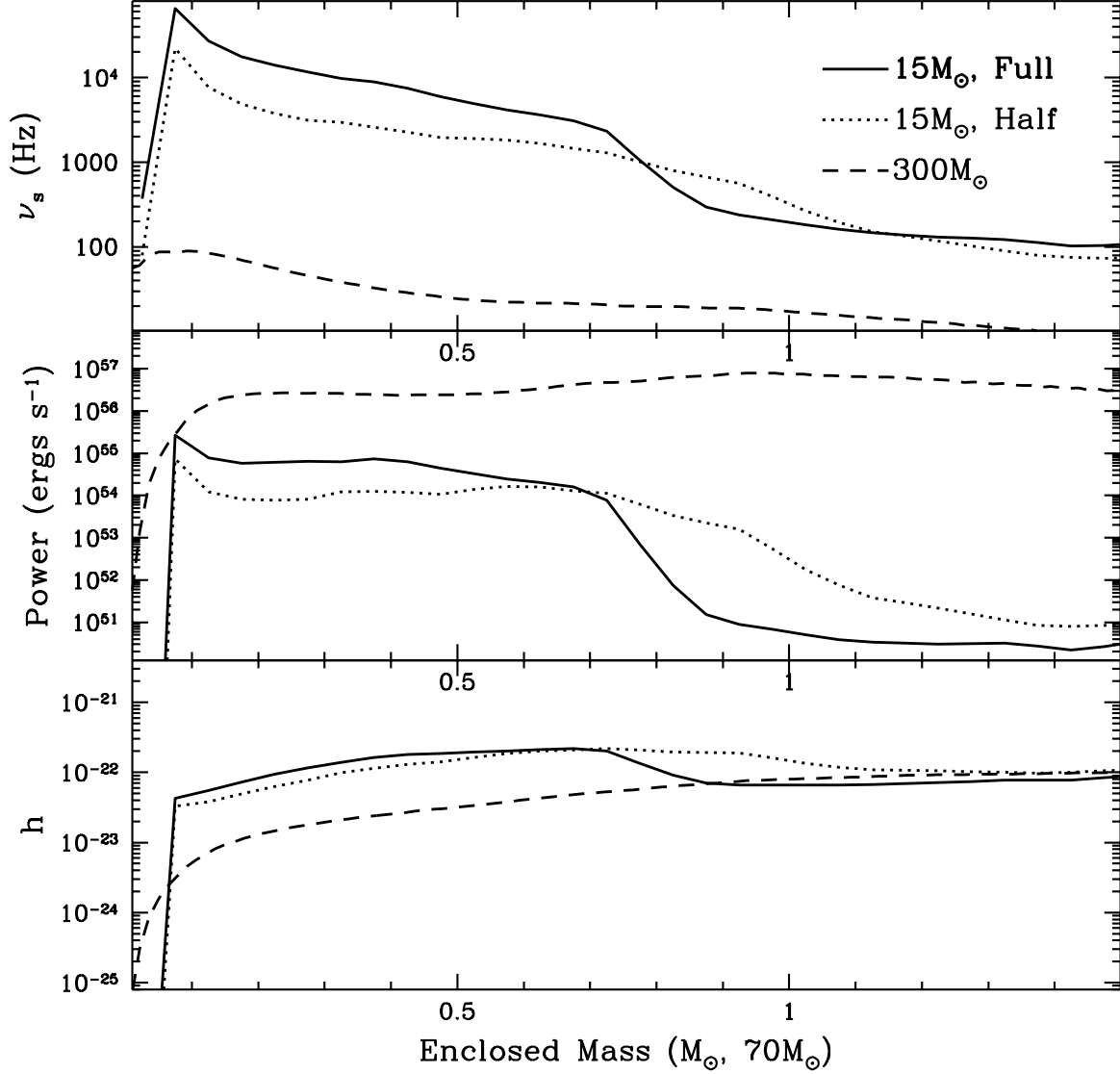


Fig. 10.— Binary spin period, power, and strain versus the mass which is converted into binaries. It is unlikely that the mass will indeed fragment into binaries, so these calculations provide a reasonably secure upper limit for the GW emission from stellar collapse. The strain is calculated assuming a distance of 10 Mpc for the 15 M_\odot collapse simulations, and $z = 10$ for the 300 M_\odot simulations.

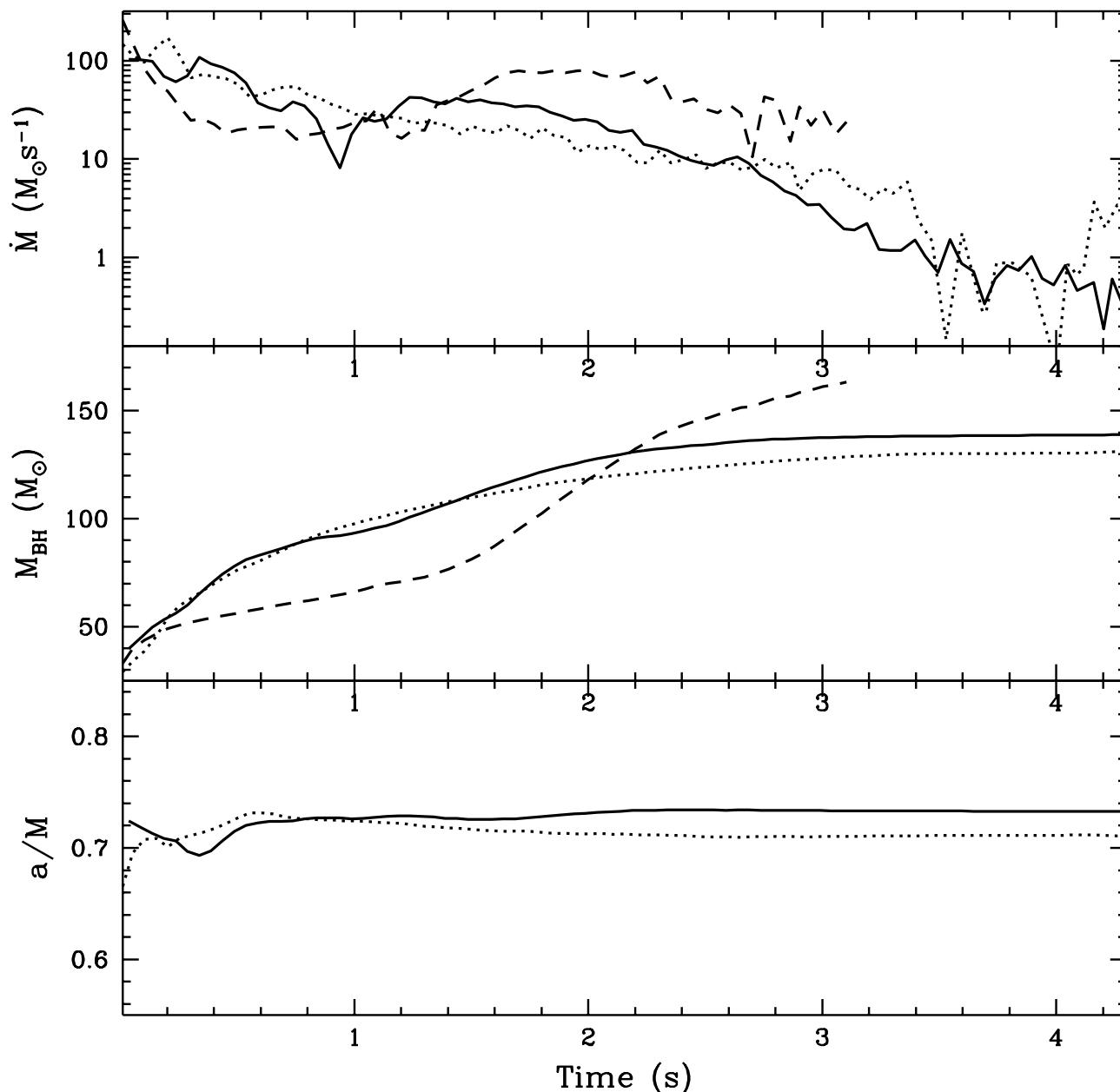


Fig. 11.— Accretion rate, black hole mass, and black hole spin versus time after black hole formation in the collapse of a $300 M_{\odot}$ star. The dashed line assumes no angular momentum, and the dotted and solid lines assume the angular momentum derived in stellar evolution models (see Fryer et al. 2001) with and without angular momentum transport, respectively. The strain is calculated assuming a distance of 10 Mpc for the $15 M_{\odot}$ collapse simulations, and $z = 10$ for the $300 M_{\odot}$ simulation.